

# Reconciling Contrasting Relationships Between Relative Dispersion and Volume-Mean Radius of Cloud Droplet Size Distributions

Chunsong Lu<sup>1</sup> , Yangang Liu<sup>2</sup> , Seong Soo Yum<sup>3</sup> , Jingyi Chen<sup>4</sup> , Lei Zhu<sup>1</sup>, Sinan Gao<sup>1</sup>, Yan Yin<sup>1</sup> , Xingcan Jia<sup>5</sup> , and Yuan Wang<sup>1</sup> 

<sup>1</sup>Collaborative Innovation Center on Forecast and Evaluation of Meteorological Disasters (CIC-FEMD) and Key Laboratory for Aerosol-Cloud-Precipitation of China Meteorological Administration, Nanjing University of Information Science and Technology, Nanjing, China, <sup>2</sup>Environmental and Climate Sciences Department, Brookhaven National Laboratory, Upton, NY, USA, <sup>3</sup>Department of Atmospheric Sciences, Yonsei University, Seoul, South Korea, <sup>4</sup>Pacific Northwest National Laboratory, Richland, WA, USA, <sup>5</sup>Institute of Urban Meteorology, China Meteorological Administration, Beijing, China

**Key Points:**

- The correlation between relative dispersion and volume-mean radius changes from positive to negative with increasing volume-mean radius
- A hypothesis is proposed to relate positive/negative correlations to microphysical processes
- This hypothesis is substantiated with numerical simulations and theoretical derivation

**Correspondence to:**

C. Lu and Y. Liu,  
luchunsong110@gmail.com;  
lyg@bnl.gov

**Citation:**

Lu, C., Liu, Y., Yum, S. S., Chen, J., Zhu, L., Gao, S., et al. (2020). Reconciling contrasting relationships between relative dispersion and volume-mean radius of cloud droplet size distributions. *Journal of Geophysical Research: Atmospheres*, 125, e2019JD031868. <https://doi.org/10.1029/2019JD031868>

Received 20 OCT 2019

Accepted 1 APR 2020

Accepted article online 16 APR 2020

**Abstract** Cloud droplet spectral relative dispersion is critical to parameterizations of cloud radiative properties, warm-rain initiation, and aerosol-cloud interactions in models; however, there is no consistent relationship between relative dispersion and volume-mean radius in literature, which hinders improving relative dispersion parameterization and calls for physical explanation. Here we show, by analyzing aircraft observations of cumulus clouds during Routine AAF [Atmospheric Radiation Measurement (ARM) Aerial Facility] Clouds with Low Optical Water Depths (CLOWD) Optical Radiative Observations, that the correlation between relative dispersion and volume-mean radius changes from positive to negative as volume-mean radius increases. With the new observation, we postulate that the sign of the correlation is determined by whether or not condensation (evaporation) occurs simultaneously with significant new activation (deactivation). The hypothesis is validated by simulations of both an adiabatic cloud parcel model and a parcel model accounting for entrainment-mixing. A new quantity, first bin strength, is introduced to quantify this new observation. Theoretical analysis of truncated gamma and modified gamma size distributions further supports the hypothesis and reconciles the contrasting relationships between relative dispersion and volume-mean radius, including the results in polluted fog observations. The results could shed new light on the so-called “twilight zone” between cloudy and cloud-free air, which in turn affects evaluation of aerosol-cloud interactions and retrieval of aerosol optical depth.

**Plain Language Summary** The width of cloud droplet size distribution is critical to aerosol-cloud interactions and warm rain initiation. Relative dispersion represents the relative width of cloud droplet size distribution. Current parameterizations of relative dispersion often relate relative dispersion to volume-mean radius. Based on aircraft observations of cumulus clouds, it is found that relative dispersion is positively correlated with volume-mean radius when volume-mean radius is small, and the correlation becomes negative when volume-mean radius increases. A hypothesis is raised by relating the relationship between the two quantities to microphysical processes (activation, condensation, evaporation, and deactivation) and is substantiated with an adiabatic parcel model, a parcel model considering entrainment-mixing, and theoretical analysis. The results may promote the studies on the zone between cloudy and cloud-free air, which in turn affects evaluation of aerosol-cloud interactions.

## 1. Introduction

Clouds play important roles in the Earth's climate system through aerosol-cloud interactions, cloud-radiation feedbacks, and so forth (e.g., Li et al., 2017; Zhang et al., 2013). Due to the coarse grid size of general circulation models, many cloud processes are parameterized (e.g., Wang & Penner, 2010). One of the key factors in the cloud microphysics parameterizations is relative dispersion ( $\epsilon$ ), defined as the ratio of standard deviation of droplet radius to mean droplet radius of droplet size distributions. It is well known that  $\epsilon$  has significant influences on aerosol indirect effect evaluation, warm-rain initiation, cloud-climate feedbacks, through its effects on cloud effective radius, cloud optical depth (Anil Kumar et al., 2016;

McComiskey et al., 2009; Peng et al., 2007; Tas et al., 2012; Wang et al., 2011; Wang et al., 2013; Zhao et al., 2006; Zhao et al., 2019), and autoconversion processes (Liu et al., 2004; Liu et al., 2006; Liu et al., 2007; Lu et al., 2018).

In the search for ways to parameterize  $\varepsilon$  or effective radius ratio ( $\beta$ ), relationships of  $\varepsilon$  or  $\beta$  to cloud droplet number concentration ( $n_c$ ) or aerosol number concentration ( $n_a$ ) have been studied intensively;  $\beta$  is the ratio of effective radius to volume-mean radius ( $r_v$ ). Positive correlations (Anil Kumar et al., 2016; Liu & Daum, 2002; Martin et al., 1994; McFarquhar & Heymsfield, 2001; Pandithurai et al., 2012; Prabha et al., 2012; Wood, 2000; Yum & Hudson, 2005), negative correlations (Chandrakar et al., 2016; Chandrakar et al., 2018; Desai et al., 2018; Desai et al., 2019; Ma et al., 2010), and no correlations (Zhao et al., 2006) have been all found based on in situ observations or cloud chamber experiments. One important reason for these different correlations is that  $\varepsilon$  and  $n_c$  are sensitive to many factors, such as turbulent fluctuations, aerosol properties, and vertical velocity ( $w$ ) (Chandrakar et al., 2016; Liu et al., 2006; Lu et al., 2012b; Peng et al., 2007). Based on many experiments in a turbulent cloud chamber, Chandrakar et al. (2016, 2018) and Desai et al. (2018) concluded that increasing  $n_a$  ( $n_c$ ) decreased  $\varepsilon$ . The reason was that, for a higher  $n_c$ , the cloud was in a fast microphysics regime and supersaturation fluctuation was reduced; all droplets were expected to have similar condensation growth histories, resulting in smaller  $\varepsilon$ . Pawlowska et al. (2006) found that flight-averaged  $\varepsilon$  seemed to increase with  $n_c$ , consistent with theoretical expectation (Liu, Daum, & Yum, 2006). However, the correlation between the two quantities was negative within each flight, which could be due to the dominant effect of  $w$  (Liu, Daum, & Yum, 2006). With a parcel model, Chen et al. (2016, 2018) found that, for a given  $w$ ,  $\varepsilon$  increased with increasing  $n_a$  in the aerosol-limited regime, peaked in the transitional regime, and decreased with increasing  $n_a$  in the  $w$ -limited regime.

Many studies have been focusing on the effects of  $\varepsilon$  on radiative transfer and precipitation in models, using different parameterizations of  $\varepsilon$  (Peng & Lohmann, 2003; Rotstayn & Liu, 2003; Xie et al., 2017; Xie & Liu, 2011). By implementing different parameterizations of  $\varepsilon$ - $n_c$  in the Weather Research and Forecast model, Xie et al. (2013) found that the sign of the surface precipitation response induced by aerosols was dependent on the  $\varepsilon$ - $n_c$  relationships, which influenced the autoconversion processes. For a positive (negative)  $\varepsilon$ - $n_c$  correlation, the domain-averaged cumulative precipitation increased (decreased) with aerosol concentrations from maritime to continental backgrounds. Peng and Lohmann (2003) applied a positive  $\beta$ - $n_c$  relationship to a general circulation model; the results indicated that, considering the dispersion effect, the global mean indirect aerosol effect at the top of atmosphere was reduced by  $0.2 \text{ W m}^{-2}$ . With positive  $\varepsilon$ - $n_c$  relationships in different general circulation models, Rotstayn and Liu (2003) and Xie et al. (2017) also found that the aerosol indirect effects were significantly reduced.

Besides  $\varepsilon$  versus  $n_c$  ( $n_a$ ), the relationship between  $\varepsilon$  and  $r_v$ , the equivalent relationship between  $\beta$  and water per droplet ( $\gamma$ ), and also the relationship between  $\varepsilon$  and  $\gamma$  are suggested for parameterization of  $\varepsilon$  (Liu et al., 2008; Tas et al., 2012), which is thought to be better than  $\varepsilon$  versus  $n_c$  ( $n_a$ ) (Liu et al., 2008; Wood, 2000) due to their consideration of covariations in  $n_c$  and liquid water content (LWC). Similarly, both negative correlations (Liu et al., 2008; Pandithurai et al., 2012; Wood, 2000) and positive correlations (Tas et al., 2012) have been found from observations and/or simulations. Rotstayn and Liu (2009) applied two relationships of  $\beta$ - $\gamma$  (Liu et al., 2008) and  $\beta$ - $n_c$  (Liu & Daum, 2002) in a general circulation model; the scheme with  $\beta$ - $\gamma$  gave a stronger increase of  $\beta$  with increasing  $n_c$  and offset the aerosol indirect effect more strongly than the scheme with  $\beta$ - $n_c$ .

The diverse relationships between  $\varepsilon$  and  $n_c$  ( $n_a$ ) and between  $\varepsilon$  and  $r_v$ , indicate that our understanding on the factors affecting  $\varepsilon$  is far from complete, hindering parameterization of  $\varepsilon$ . More observational, numerical, and theoretical analyses are needed for a better understanding and parameterization of  $\varepsilon$ .

This study focuses on the new relationship between  $\varepsilon$  and  $r_v$  and the underlying physical mechanisms. Section 2 analyzes the aircraft observations of cumulus clouds during the Routine AAF [Atmospheric Radiation Measurement (ARM) Aerial Facility] Clouds with Low Optical Water Depths (CLOWD) Optical Radiative Observations (RACORO) field campaign, which operated over the ARM Southern Great Plains site near Lamont, Oklahoma, from 22 January to 30 June 2009 (Vogelmann et al., 2012). Plausible physical mechanisms are proposed to explain the new observational relationship between  $\varepsilon$  and  $r_v$ .

Section 3 presents numerical simulations and theoretical analysis to illustrate the proposed mechanisms. Concluding remarks are given in section 4.

## 2. New Observational Results and Underlying Physical Mechanisms

### 2.1 Observational Results in Cumulus Clouds

During RACORO, the Twin Otter aircraft from the Center for Interdisciplinary Remotely-Piloted Aircraft Studies was used to measure aerosol, cloud, meteorological information, and so forth (Vogelmann et al., 2012). The cloud droplet size distributions were measured by the Cloud and Aerosol Spectrometer probe that covers radius range from 0.29 to 25  $\mu\text{m}$  in 20 bins at 10 Hz, manufactured by Droplet Measurement Technologies (Baumgardner et al., 2001). The aircraft flew at the speed of  $\sim 50 \text{ m s}^{-1}$ ; thus, the spatial resolution of droplet size distributions is  $\sim 5 \text{ m}$ . Cloud microphysical properties are calculated only for the bins with the criterion of droplet average radii larger than 1  $\mu\text{m}$ , which has also been widely used in previous studies (Bera et al., 2016; Hsieh et al., 2009; Ma et al., 2010; Small et al., 2013; Yum et al., 2015). Another criterion used to define cloud droplets is based on whether the particle has crossed the peak in the Kohler curve. However, data for the Kohler curve method are not available; thus, 1  $\mu\text{m}$  is used as the threshold of cloud droplet. Droplets in the range of 7.50 to 781  $\mu\text{m}$  (radius) were measured by the Cloud Imaging Probe at 1 Hz. The Differential Mobility Analyzer recorded aerosol particles with radius between 0.006 and 0.3  $\mu\text{m}$  roughly once per minute. The Passive Cavity Aerosol Spectrometer Probe measured aerosols in the range of 0.05–1.12  $\mu\text{m}$  (radius) at 1 Hz. The Diode Laser Hygrometer (Diskin et al., 2002; Podolske et al., 2003) and a Rosemount probe were used to measure water vapor mixing ratio and temperature at 10 Hz, respectively. Cloud droplet size distributions satisfying both criteria of  $\text{LWC} > 0.001 \text{ g m}^{-3}$  and  $n_c > 10 \text{ cm}^{-3}$  are considered to be cloud records (Deng et al., 2009). A criterion that the in-cloud mean drizzle  $\text{LWC}$  (radius  $> 25 \mu\text{m}$  from the CIP)  $< 0.005 \text{ g m}^{-3}$  is used to identify nondrizzling clouds. Nondrizzling cumulus clouds from eight flights along horizontal legs are analyzed for the following dates: 22 May, 23 May, 24 May, 11 June, 19 June, 23 June, 24 June, and 26 June 2009.

The cumulus clouds are shallow with thicknesses mainly in the range of 200–500 m (Vogelmann et al., 2012). By use of the same methods in Liu et al. (2008) and Tas et al. (2012), microphysical properties, including  $\epsilon$  and  $r_v$ , are calculated. Briefly, the mean and standard deviation of  $\text{LWC}$ ,  $n_c$ ,  $\epsilon$ , and  $r_v$ , are  $0.16 \pm 0.18 \text{ g m}^{-3}$ ,  $652.6 \pm 459.2 \text{ cm}^{-3}$ ,  $0.35 \pm 0.11$ ,  $3.64 \pm 1.01 \mu\text{m}$ , respectively. Based on D. Baumgardner (personal communication, February 18, 2020), the Poisson sampling theory is used to estimate expected error (standard error, SE). The Cloud and Aerosol Spectrometer has a sample area of  $0.24 \text{ mm}^2$ , so the sample volume for 10 Hz is  $0.24 \text{ mm}^2 * 5 \text{ m} = 1.2 \text{ cm}^3$ , and SE is

$$SE = \frac{1}{\sqrt{n_c * 1.2}}, \quad (1)$$

For  $n_c = 652.6 \text{ cm}^{-3}$ , SE is 3.6%; for  $n_c = 652.6 - 459.2 = 193.4 \text{ cm}^{-3}$ , SE is 6.6%. Even if  $10 \text{ cm}^{-3}$  (the criterion for selecting clouds) is taken to be  $n_c$ , SE is 28.9%, still smaller than 30%. Therefore, 5 m is a reasonable length to obtain a statistically significant droplet size distribution.

Figure 1a shows that  $\epsilon$  and  $r_v$  are positively correlated when  $r_v \leq 2.2 \mu\text{m}$  but become negatively correlated when  $r_v > 2.2 \mu\text{m}$ . To clearly show the relationship, the frequency distribution for  $r_v > 2.2 \mu\text{m}$  is also added. The branch of negative correlation is consistent with the results shown in Wood (2000), Liu et al. (2008), and Pandithurai et al. (2012); the branch of positive correlation is consistent with the previous study by Tas et al. (2012). Compared with this study, these studies used similar instruments or had similar ranges of cloud droplet sizes. Therefore, the comparisons between this study and the previous studies are valid. To the authors' knowledge, such a nonmonotonic variation of the correlation between  $\epsilon$  and  $r_v$  has not been reported so far.

To help understand the reason why the sign of the correlation between  $\epsilon$  and  $r_v$  changes, Figure 1b compares the mean cloud droplet size distributions for the groups of  $r_v \leq 2.2$  and  $r_v > 2.2 \mu\text{m}$ . Evidently, the peak of the mean cloud droplet size distribution is at the first bin ( $\sim 1 \mu\text{m}$ , i.e., a significantly truncated size distribution) for the  $r_v \leq 2.2 \mu\text{m}$  group but around 3  $\mu\text{m}$  for the  $r_v > 2.2 \mu\text{m}$  group. To further quantify the difference between the two groups, we define the first bin strength (FBS):

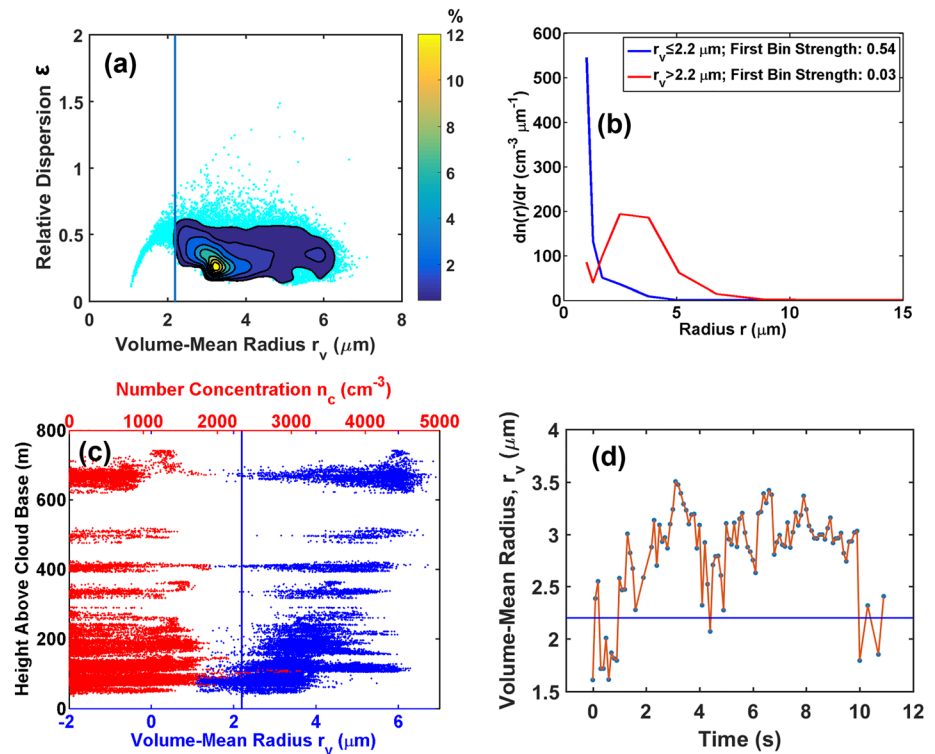


**Figure 1.** (a) Relative dispersion ( $\epsilon$ ) as a function of volume-mean radius ( $r_v$ ) in the cumulus clouds during RACORO. The frequency distribution for  $r_v > 2.2 \mu\text{m}$  is also added. (b) Cloud droplet size distributions ( $dn(r)/dr$ ) in different  $r_v$  ranges;  $r$  is droplet radius, and  $n$  ( $r$ ) is number concentration for the bin of  $r$ . First bin strength is also shown in the legend. (c) Number concentration ( $n_c$ ) and  $r_v$  as a function of height above cloud base. (d)  $r_v$  as a function of time in a typical cloud on 23 May 2009 (one example). The solid straight lines in (c) and (d) represent  $r_v$  equal to  $2.2 \mu\text{m}$ .

$$FBS = \frac{n_1}{n_c}, \quad (2)$$

where  $n_1$  is the first bin number concentration. Larger FBS corresponds to more likelihood of having peak at/close to the first bin. FBS is 0.54 for the group of  $r_v \leq 2.2 \mu\text{m}$ , much larger than 0.03 for the group of  $r_v > 2.2 \mu\text{m}$ .

## 2.2 Plausible Physical Mechanisms

To help understand the physical processes underlying the two groups, Figure 1c shows  $n_c$  and  $r_v$  as a function of height above cloud base in all cumulus clouds in RACORO. Along each horizontal leg, there are some growing cumulus clouds. The maximum LWC within a cumulus cloud is assumed to be adiabatic LWC. The cloud base for each growing cumulus cloud is estimated based on the adiabatic LWC. A cloud parcel with the adiabatic LWC moves downward until LWC is equal to 0 (cloud base). The uncertainty of this method has been discussed in Lu et al. (2012a). Many other methods have been used for cloud base height estimation. For example, cloud base can be estimated as the cloud condensation level using meteorological information in the boundary layer or near surface (Wallace & Hobbs, 2006). Gerber et al. (2008) and Lu et al. (2012) fitted maximum LWC at different heights from aircraft observations with a linear profile to estimate cloud base. Some instruments, such as lidar, are often used to determine cloud base (Clothiaux et al., 2000). However, there were significant spatial changes in cloud base heights even during one flight in RACORO (Vogelmann et al., 2012), so these methods are not applicable. After cloud base is determined for each cloud, all the cloud base heights along one aircraft horizontal leg are averaged and taken to be the cloud base height along that leg. As shown in Figure 1c,  $n_c$  does not vary much with height; the data points with  $r_v \leq 2.2 \mu\text{m}$  are present at all heights, but most of them are near the cloud base. Figure 1d shows an example of  $r_v$  as a

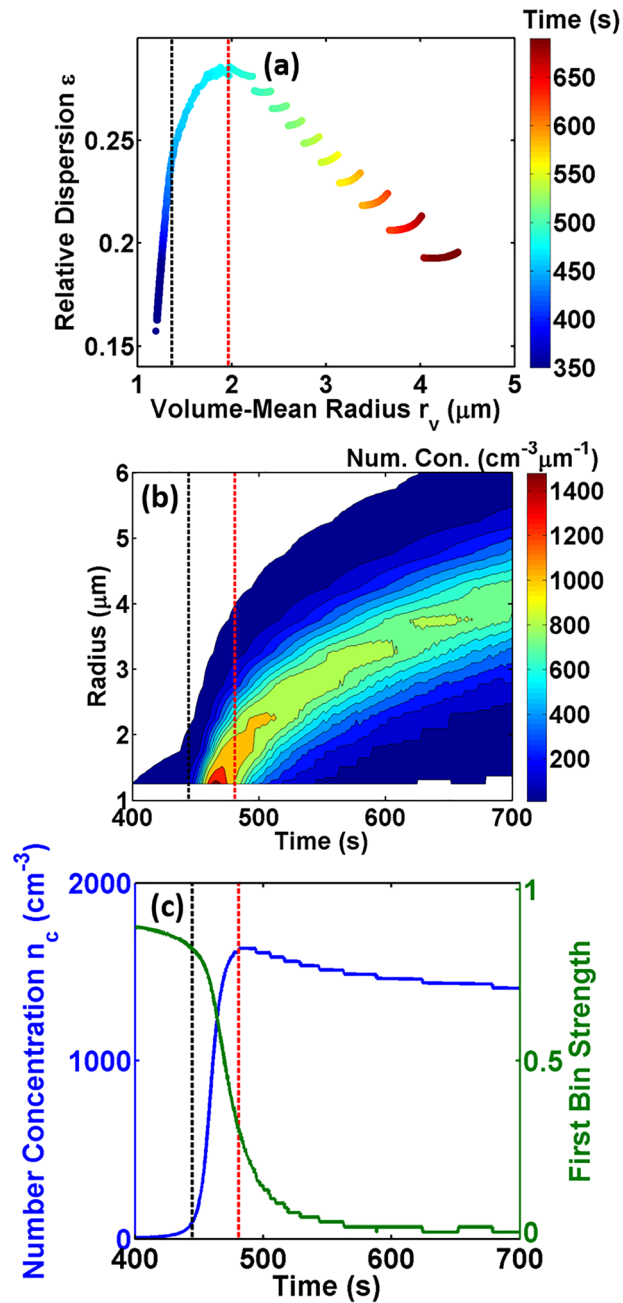


**Figure 2.** (a) Relative dispersion ( $\epsilon$ ) as a function of volume-mean radius ( $r_v$ ), (b) temporal evolution of cloud droplet size distributions, and (c) temporal evolution of number concentration ( $n_c$ ) during the adiabatic growing process simulated by a parcel model with  $r_{\text{aerosol}}$  of  $0.032 \mu\text{m}$ ,  $\sigma_{\text{aerosol}}$  of  $2.02$  in equation 3, and vertical velocity of  $0.81 \text{ m s}^{-1}$ . The red line represents the maximum  $\epsilon$ ; the black line represents the criteria of liquid water content (LWC) equal to  $0.001 \text{ g m}^{-3}$  and  $n_c$  equal to  $10 \text{ cm}^{-3}$ .

function of time in a typical cloud on 23 May 2009; many data points with  $r_v \leq 2.2 \mu\text{m}$  in the individual cloud are near the cloud edges.

Liu et al. (2008) argued that condensation was responsible for the negative  $\epsilon$ - $r_v$  correlation. Tas et al. (2012) attributed the positive  $\epsilon$ - $r_v$  correlation to the impact of collision-coalescence. The nondrizzling clouds analyzed here are weakly, if any, affected by collision-coalescence. Based on the fact that the branch of positive  $\epsilon$ - $r_v$  correlation is associated with the peak radius at the first bin and the measurements are near the cloud

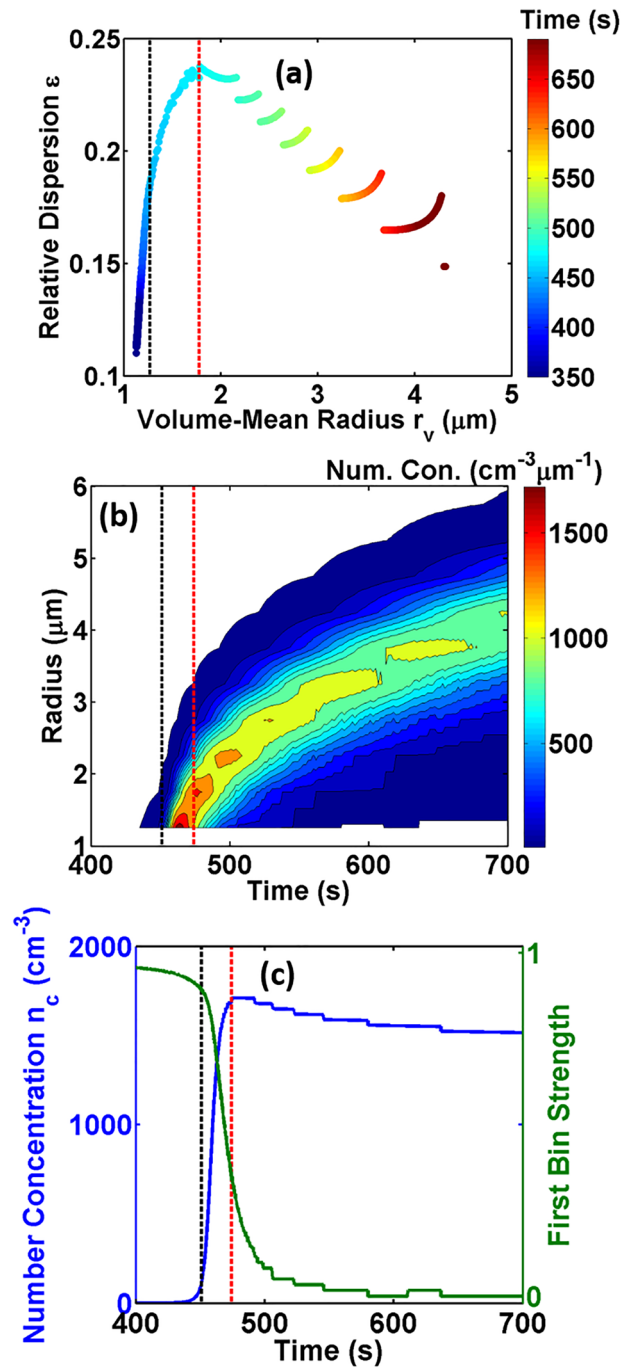


**Figure 3.** Same as Figure 2 but for  $r_{aerosol}$  equal to  $0.032 \mu\text{m}$  and  $\sigma_{aerosol}$  equal to 1.78 in equation 3.

boundary where condensation and new droplet activation, or evaporation and droplet deactivation, likely occur simultaneously, we propose new mechanisms: Whether the correlation is positive or negative is related to whether condensation occurs simultaneously with significant new droplet activation and/or whether evaporation occurs with significant droplet deactivation.

As mentioned above, the positive correlation is generated by the data collected mainly near the cloud base in the earlier formation stage and/or near the cloud edge in the dissipation stage, where LWC is small. The negative correlation is generated from the data collected in developing and mature stages of cloud when

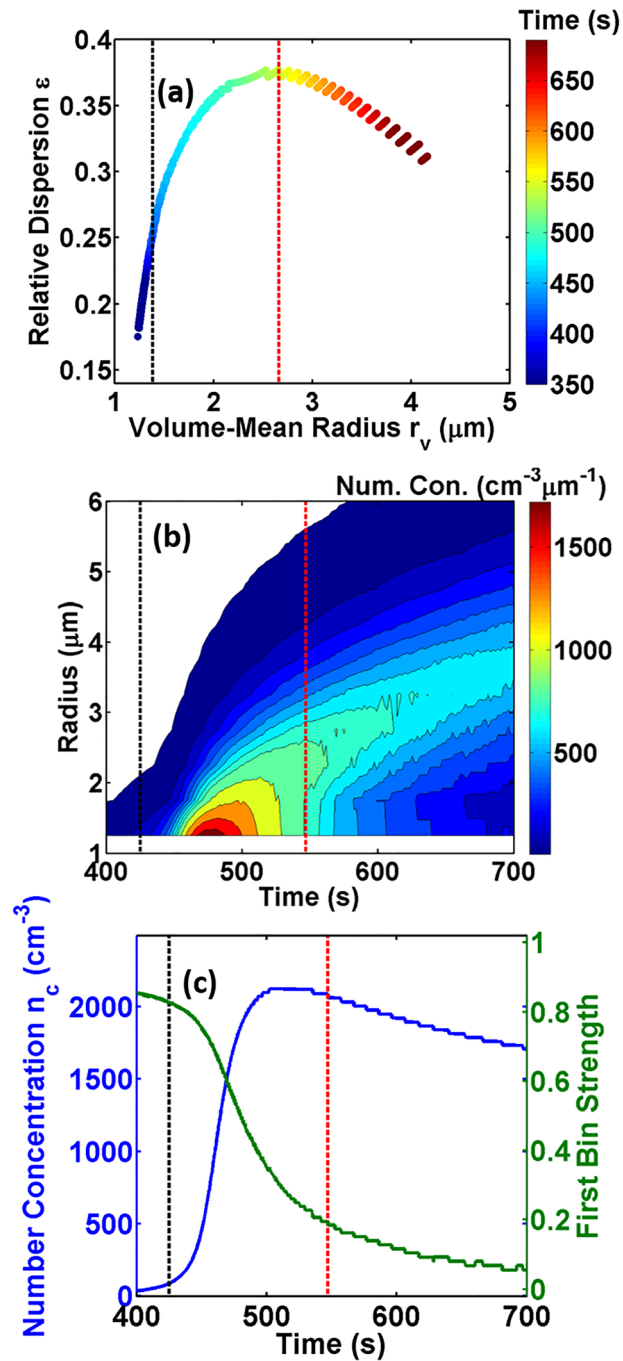


**Figure 4.** Same as Figure 2 but for  $r_{\text{aerosol}}$  equal to  $0.047 \mu\text{m}$  and  $\sigma_{\text{aerosol}}$  equal to 2.02 in equation 3.

condensation and entrainment-mixing are active; therefore, a large variation of LWC exists among different cloud parcels. As a result,  $r_v$  for the positive correlation ranges from  $\sim 1.5$  to  $2.2 \mu\text{m}$  and the negative correlation has a much wider range of  $r_v$  starting from  $2.2 \mu\text{m}$ . Therefore, the data scatter is wide and the correlation is weak for the negative correlation. (Figure 1a).

### 3. Validation of the Hypothesis

Here the temporal variations of cloud microphysics in the parcel models are used to validate the hypothesis raised based on spatial variations (Figure 1). This is valid because the cumulus observations include clouds

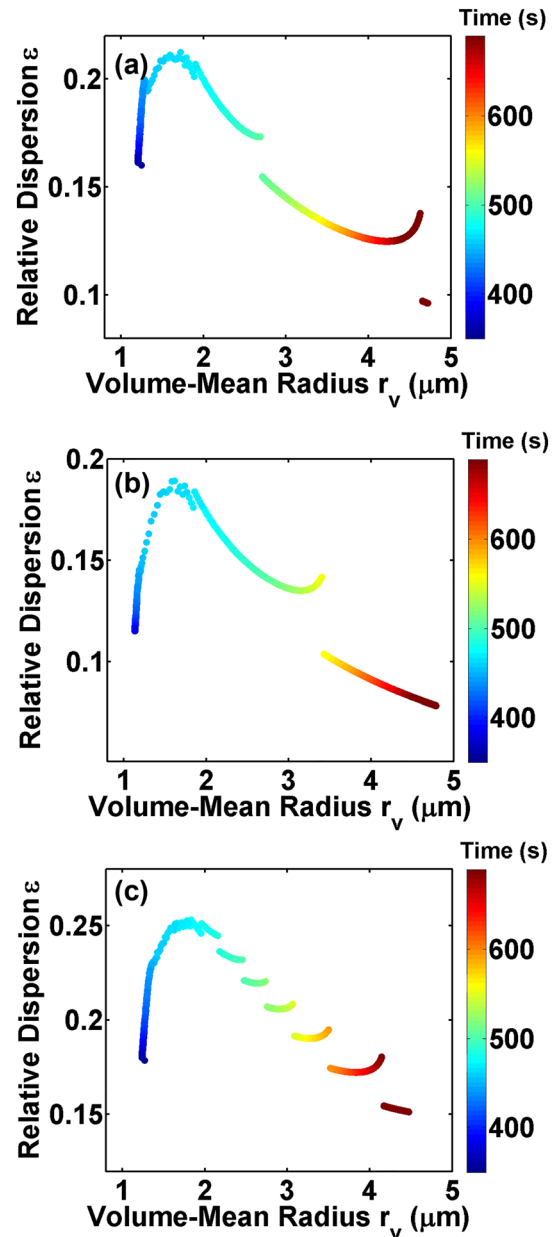


**Figure 5.** Relative dispersion ( $\epsilon$ ) as a function of volume-mean radius ( $r_v$ ) assuming biomass burning aerosols. (a)  $r_{\text{aerosol}}$  equals  $0.032 \mu\text{m}$  and  $\sigma_{\text{aerosol}}$  equals  $2.02$  in equation 3. (b)  $r_{\text{aerosol}}$  equals  $0.032 \mu\text{m}$  and  $\sigma_{\text{aerosol}}$  equals  $1.78$ . (c)  $r_{\text{aerosol}}$  equals  $0.047 \mu\text{m}$  and  $\sigma_{\text{aerosol}}$  equals  $2.02$ . Vertical velocity is  $0.81 \text{ m s}^{-1}$ .

in different stages at different heights above cloud bases. Different clouds are affected by activation, condensation, evaporation, and deactivation to different extents. From the ensemble perspective, observed spatial variation would be equivalent to temporal variation of the model result.

### 3.1 Condensation With/Without Significant New Droplet Activation

As discussed above, concurrent occurrence of condensation and droplet activation could be one reason responsible for the group of  $r_v \leq 2.2 \mu\text{m}$ . To support this hypothesis, an adiabatic cloud parcel model (Chen et al., 2016, 2018) is used to examine the effect of activation of aerosol on the correlation between  $\epsilon$  and  $r_v$  during the formation and growth of an adiabatic cloud. This model follows the “Lagrangian bin” and contains full treatment of cloud droplet nucleation and condensation (Howell, 1949). Supersaturation

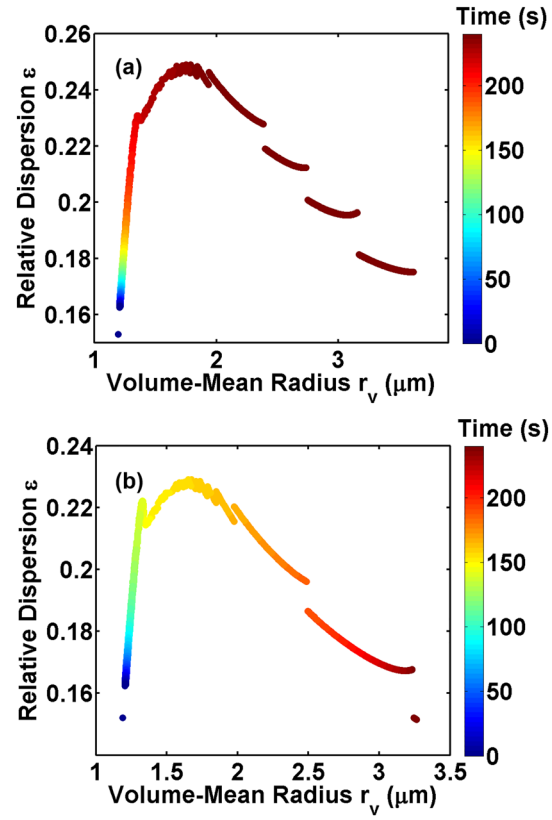


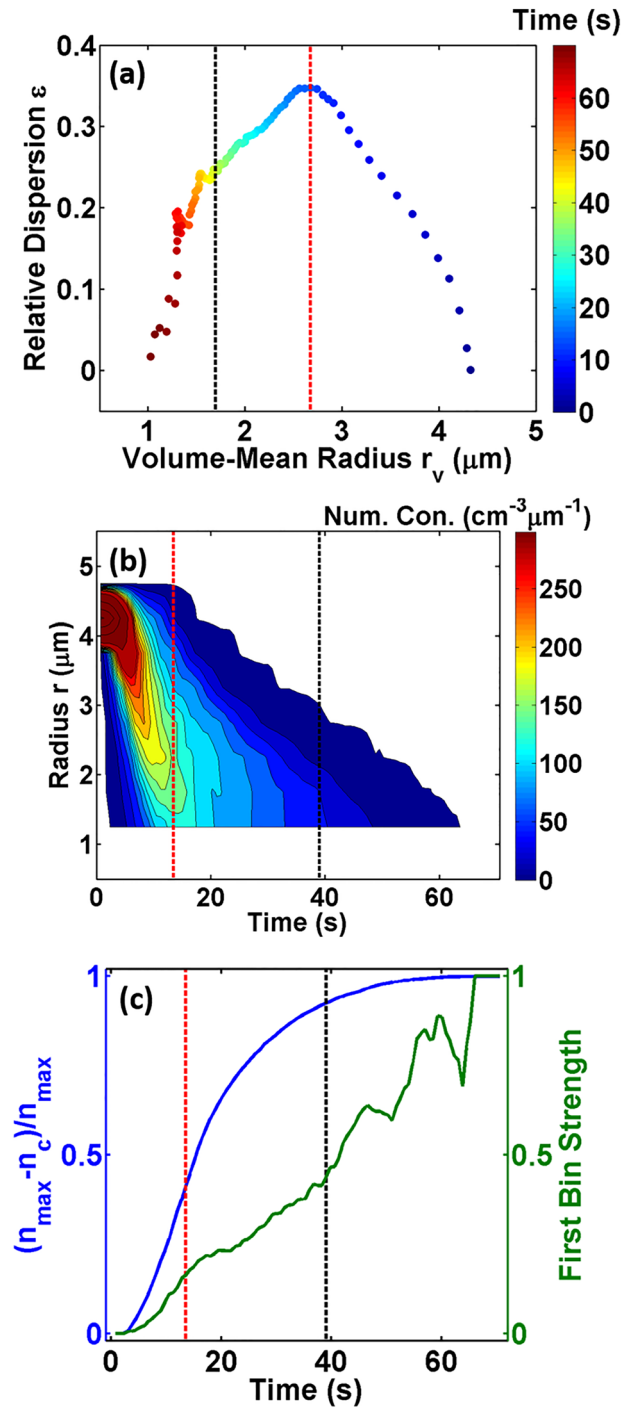
**Figure 6.** Relative dispersion ( $\epsilon$ ) as a function of volume-mean radius ( $r_v$ ) simulated by a parcel model with  $r_{aerosol}$  equal to  $0.032 \mu\text{m}$ ,  $\sigma_{aerosol}$  equal to 2.02 in equation 3, and vertical velocity equal to (a)  $1.66$  and (b)  $2.51 \text{ m s}^{-1}$ , respectively.

is produced due to adiabatic upward movement of the cloud parcel. Under the condition of supersaturation, aerosols activate and cloud droplets grow according to the condensational growth equation. Aerosol activation is treated by the  $\kappa$ -Kohler method (Petters & Kreidenweis, 2007). This model does not consider entrainment-mixing or collision-coalescence. The aerosol particles and cloud droplets are divided into 1,000 bins. The simulation is initialized with the RACORO measurements. The cloud base heights are determined by assuming that the maximum LWC in each cloud is the adiabatic LWC, as discussed above (Lu, Liu, Niu, & Vogelmann, 2012a). In five out of the eight flights (22–24 May and 11 and 19 June), there were horizontal legs below cloud base; the meteorological and aerosol information along the nearest horizontal flight leg below cloud base in these five flights are averaged and taken as the input to the model. Air temperature, pressure, and relative humidity are 291.4 K, 888.8 hPa, and 83.9%, respectively. The initial aerosol size distribution is assumed to be a lognormal distribution:

$$\frac{dn_{aerosol}}{d\log r_{aerosol}} = \frac{N_t}{(2\pi)^{1/2} \log \sigma_{aerosol}} \exp\left(-\frac{(\log r_{aerosol} - \log r_{aerosol}^-)^2}{2 \log^2 \sigma_{aerosol}}\right), \quad (3)$$

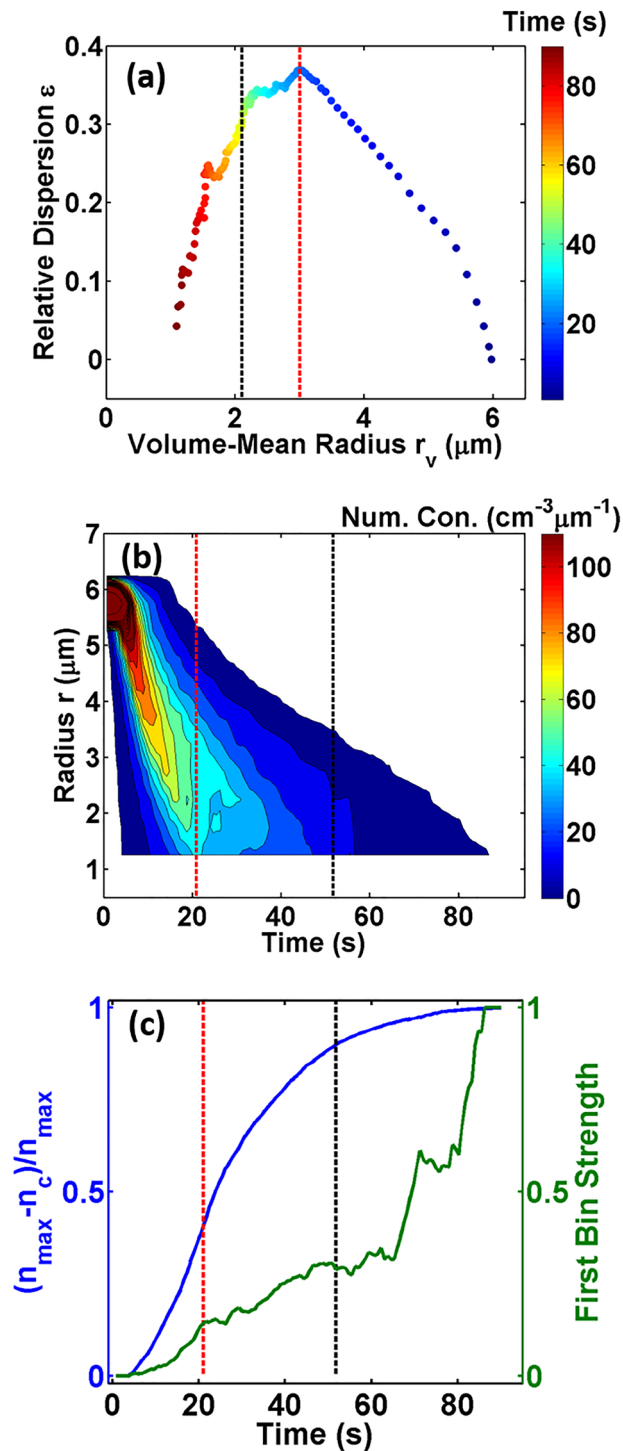
where  $n_{aerosol}$  is aerosol number concentration for bin radius of  $r_{aerosol}$ ; the mean value of  $N_t$ ,  $r_{aerosol}$ , and  $\sigma_{aerosol}$  are  $13,391 \text{ cm}^{-3}$ ,  $0.032 \mu\text{m}$ , and 2.02, respectively, based on the aerosol observations from the Passive Cavity Aerosol Spectrometer Probe and Differential Mobility Analyzer. The aerosols are assumed to be ammonium sulfate. The mean  $w$  is  $0.81 \text{ m s}^{-1}$ , calculated with all clouds along the horizontal legs in the eight flights.

Figure 2a shows that, as  $r_v$  increases, the correlation between  $\epsilon$  and  $r_v$  changes from positive to negative at  $r_v \sim 2 \mu\text{m}$ . The red dash line represents the time (481 s) when the sign change occurs. Since the parcel



**Figure 7.** (a) Relative dispersion ( $\varepsilon$ ) as a function of volume-mean radius ( $r_v$ ), (b) temporal evolution of cloud droplet size distributions, and (c) temporal evolution of  $(n_{\text{max}} - n_c) / n_{\text{max}}$  and first bin strength during the entrainment-mixing process simulated by the Explicit Mixing Parcel Model, where  $n_c$  is number concentration and  $n_{\text{max}}$  is the maximum value of  $n_c$ . The red line represents the maximum  $\varepsilon$ ; the black line represents the criteria of liquid water content (LWC) equal to  $0.001 \text{ g m}^{-3}$  and  $n_c$  equal to  $10 \text{ cm}^{-3}$ . Initial droplet radius, dissipation rate in cloud, and water vapor mixing ratio in environment are  $4.35 \mu\text{m}$ ,  $0.00576 \text{ m}^2 \text{ s}^{-3}$ , and  $10.6 \text{ g kg}^{-1}$ , respectively.

model follows the “Lagrangian bin” concept (Chen et al., 2016; Howell, 1949), the boundaries and widths of cloud droplet bins change with time. Here the cloud droplets with radii larger than  $1 \mu\text{m}$  are resampled to produce new size distributions with bin width of  $0.5 \mu\text{m}$ . As shown in Figure 2b, to the left of the red line,



**Figure 8.** Same as Figure 7 but for volume-mean radius equal to  $6 \mu\text{m}$ .

the peaks of droplet size distributions are mainly at the first bin. Condensation occurs simultaneously with a large number of newly activated droplets, as evidenced by the increase of  $n_c$  until 481 s (Figure 2c); the increase of  $n_c$  signals the activation intensity. In contrast, the cloud droplet size distributions to the right of the red line have their peaks in the middle of droplet size distributions (Figure 2b). This is caused by condensational growth without newly activated droplets. According to the classical condensation theory,

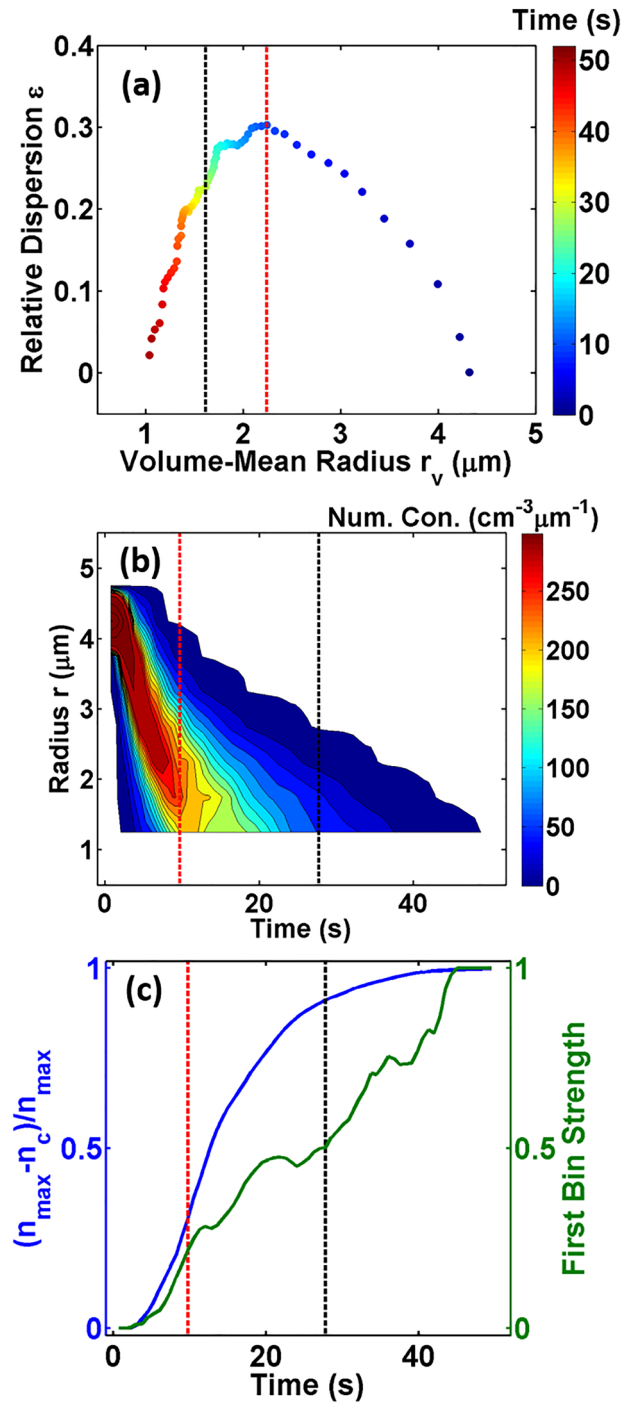
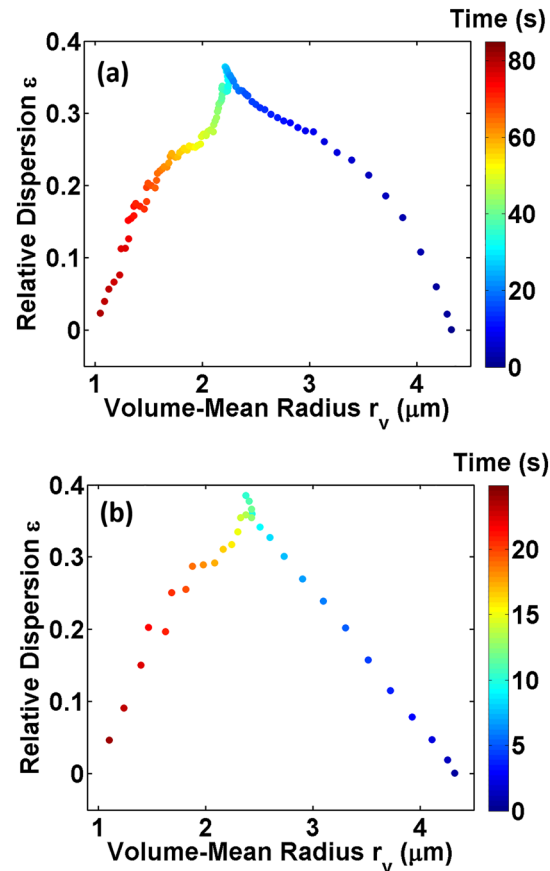


Figure 9. Same as Figure 7 but for dissipation rate equal to  $0.0576 \text{ m}^2 \text{ s}^{-3}$ .

$r_v$  increases with decreasing spectral width, for example,  $\varepsilon$  (Rogers & Yau, 1989); the truncation of cloud droplet size distribution weakens and FBS decreases with time. Therefore, condensation with (without) significant concurrent activation of new droplets could generate the positive (negative) correlation between  $\varepsilon$  and  $r_v$ . The adiabatic parcel model results support the hypothesis.

It is also interesting to find that  $n_c$  begins to decrease at 481 s due to the ripening effect (Wood et al., 2002). Small droplets need higher supersaturation to keep equilibrium than big droplets. Therefore, small droplets



**Figure 10.** Relative dispersion ( $\epsilon$ ) as a function of volume-mean radius ( $r_v$ ) during the entrainment-mixing process simulated by the Explicit Mixing Parcel Model: (a) water vapor mixing ratio of  $11 \text{ g kg}^{-1}$  in environment with 12 dry air blobs and (b) water vapor mixing ratio of  $11.4 \text{ g kg}^{-1}$  with 16 dry air blobs.

evaporate and some of them are deactivated. This ripening effect is also responsible for the discontinuous data points to the right of the red line in Figure 2a. If  $w$  is large, supersaturation would be higher than the equilibrium supersaturation for both small and big droplets. In this case, there would be no ripening effect and  $n_c$  would be constant after 481 s. Fluctuation of  $w$  could also affect the ripening effect (Wood et al., 2002). In addition, if the data points to the left of the black line ( $\text{LWC} = 0.001 \text{ g m}^{-3}$  and  $n_c = 10 \text{ cm}^{-3}$ ) are not included, the variation trend of  $\epsilon$  versus  $r_v$  does not change. Including these points, the positive correlation is more significant.

To understand the effects of  $r_{\text{aerosol}}$  and  $\sigma_{\text{aerosol}}$  on the results, sensitivity tests are carried out, assuming that  $r_{\text{aerosol}}$  and  $\sigma_{\text{aerosol}}$  are  $0.032 \pm 0.015 \mu\text{m}$  and  $2.02 \pm 0.24$ , respectively; here  $0.015 \mu\text{m}$  and  $0.24$  are the standard deviations of  $r_{\text{aerosol}}$  and  $\sigma_{\text{aerosol}}$ , respectively. The results are similar to Figure 2, and two examples are shown in Figures 3 and 4. Considering that the aerosols at the Southern Great Plains site are continental, affected by biomass burning (Fast et al., 2019), sensitivity tests are carried out assuming biomass burning aerosol. Figure 5 shows that the results are similar. In addition, the standard deviation of  $w$  is  $1.7 \text{ m s}^{-1}$ ; changing  $w$  to  $1.66 (=0.81 + 1.7/2)$  or  $2.51 (=0.81 + 1.7)$   $\text{m s}^{-1}$  does not affect the conclusions either (Figure 6).

### 3.2 Evaporation With/Without Significant Droplet Deactivation

As shown in Figure 1, many data points of  $r_v \leq 2.2 \mu\text{m}$  are near cloud edges, which are significantly affected by entrainment-mixing processes (Beals et al., 2015; Kumar et al., 2014; Lu et al., 2013). Some droplets could evaporate significantly and deactivated into interstitial aerosol particles. According to the hypothesis,

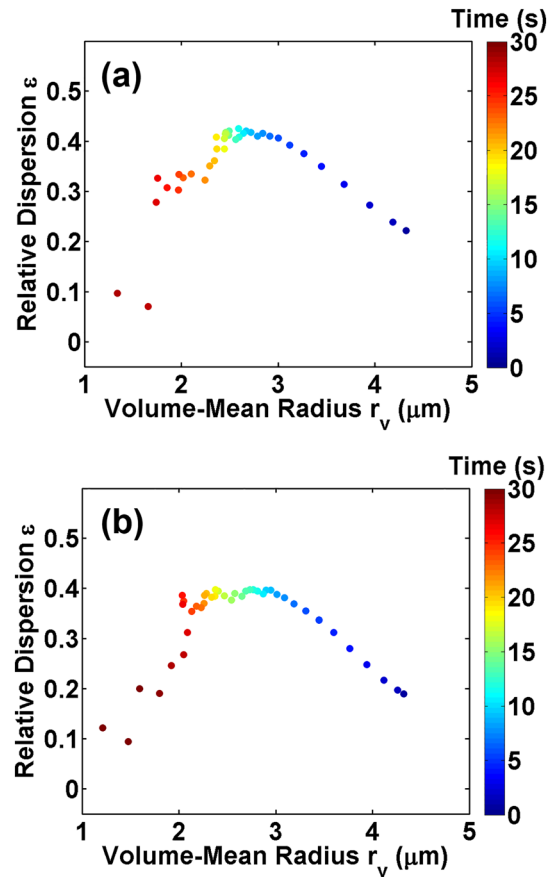


**Figure 11.** Relative dispersion ( $\epsilon$ ) as a function of volume-mean radius ( $r_v$ ) during the entrainment-mixing process simulated by the Explicit Mixing Parcel Model assuming gamma distribution: (a) parameter ( $\mu$ ) of 20.4 in equation 4, dissipation rate of  $0.0576 \text{ m}^2 \text{ s}^{-3}$ , and water vapor mixing ratio of  $11.4 \text{ g kg}^{-1}$ . (b) Parameter ( $\mu$ ) of 27.86 ( $= 20.4 + 7.46$ ), dissipation rate of  $0.00576 \text{ m}^2 \text{ s}^{-3}$ , and water vapor mixing ratio of  $11.4 \text{ g kg}^{-1}$ .

whether evaporation occurs with significant droplet deactivation could determine the sign of the correlation between  $\epsilon$  and  $r_v$ .

To substantiate this hypothesis, the Explicit Mixing Parcel Model (EMPM) (Krueger et al., 1997; Su et al., 1998) is used. The domain size of EMPM is  $20 \text{ m}$  (width)  $\times$   $0.001 \text{ m}$  (height)  $\times$   $0.001 \text{ m}$  (depth), which was used in Su et al. (1998), Lu et al. (2018), and Tölle and Krueger (2014). Krueger (2008) introduced the events/processes in the model. When entrainment occurs, the entrained dry air replaces the same-sized segment of adiabatic cloud parcel. After that, the cloudy air and dry air undergo isobaric mixing and evaporation. Many cloud droplets encounter the dry air and may evaporate partially or even deactivate.

The model setting is based on the mean states in the cumulus clouds during RACORO. The adiabatic cloud parcel is assumed to have water vapor mixing ratio ( $q_v$ ) of  $12.3 \text{ g kg}^{-1}$ , temperature of  $286.7 \text{ K}$ , and pressure of  $796.2 \text{ hPa}$ . The adiabatic LWC of  $0.46 \text{ g m}^{-3}$  is assumed to be the average value of maximum LWC in different clouds, similar to Lu, Liu, Niu, and Vogelmann (2012a). The adiabatic  $n_c$  of  $1332.6 \text{ cm}^{-3}$  is the average value of  $n_c$  corresponding to the maximum LWC, and  $r_v$  of  $4.35 \mu\text{m}$  is calculated according to the adiabatic LWC and  $n_c$ . Ten dry air blobs are entrained, and each one has a size of  $1 \text{ m} \times 0.001 \text{ m} \times 0.001 \text{ m}$  that was also used in Tölle and Krueger (2014). The entrained dry air has  $q_v$  of  $10.6 \text{ g kg}^{-1}$  and temperature of  $286.2 \text{ K}$ , which are the average values near the cloud edges. The turbulent dissipation rate is  $0.00576 \text{ m}^2 \text{ s}^{-3}$ , which is the average value within all clouds.

As shown in Figure 7,  $\epsilon$  and  $r_v$  are negatively correlated from 0 to 13.5 s (the red dash line). The reason is that some droplets evaporate faster than the others. The ratio of  $\frac{n_{\text{max}} - n_c}{n_{\text{max}}}$  can quantitatively describe the

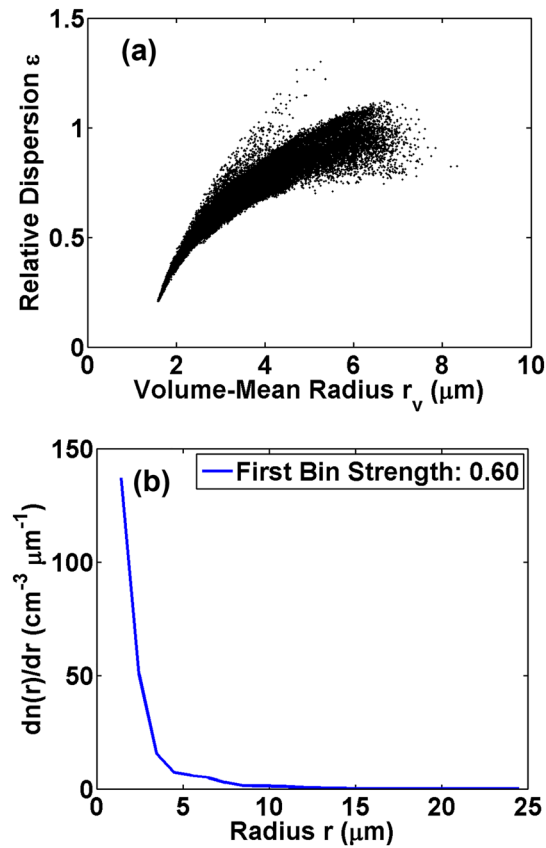


**Figure 12.** (a) Relative dispersion ( $\epsilon$ ) as a function of volume-mean radius ( $r_v$ ) and (b) mean cloud droplet size distribution in a fog case in Nanjing, China, from 16:37 BST (universal time coordinated + 8 hr) on 19 December to 16:11 BST on 20 December 2007.

deactivation process, where  $n_{\max}$  is the maximum value of  $n_c$ .  $\frac{n_{\max} - n_c}{n_{\max}}$  is smaller than 0.41 before 13.5 s, and FBS is smaller than 0.16. As a result,  $\epsilon$  increases and  $r_v$  decreases. The cloud droplet size distributions tend to have their peaks in the middle of distributions. After 13.5 s, the correlation between  $\epsilon$  and  $r_v$  becomes positive. The reason is that more and more droplets are significantly evaporated and deactivated into aerosol particles; both  $\epsilon$  and  $r_v$  decrease at the same time. Both  $\frac{n_{\max} - n_c}{n_{\max}}$  and FBS increase significantly, and the peaks of cloud droplet size distributions tend to be at the first bin. Therefore, evaporation with (without) significant deactivation can also cause a positive (negative) correlation between  $\epsilon$  and  $r_v$ , validating the hypothesis.

In addition, the black line represents the criteria of  $\text{LWC} = 0.001 \text{ g m}^{-3}$  and  $n_c = 10 \text{ cm}^{-3}$ . Even when LWC and  $n_c$  are smaller than the criteria, the correlation between  $\epsilon$  and  $r_v$  is still positive and the droplet size distribution still has its peak at the first bin. Sensitivity tests are performed by changing initial radius from 4.35 to 6  $\mu\text{m}$  and dissipation rate from 0.00576 to 0.0576  $\text{m}^2 \text{ s}^{-3}$ , respectively (Figures 8 and 9). Two other sensitivity tests are shown in Figure 10:  $q_v$  of 11  $\text{g kg}^{-1}$  in environment with 12 dry air blobs and  $q_v$  of 11.4  $\text{g kg}^{-1}$  with 16 dry air blobs, respectively. With the increasing  $q_v$  in environment, more dry air blobs are needed to satisfy the condition that evaporation occurs with significant droplet deactivation. The results are quite similar to Figure 7. In addition, a fixed droplet size is used in the above simulations. To examine the dependence of  $\epsilon$  versus  $r_v$  on the initial droplet size distribution, cloud droplet size distributions corresponding to the maximum LWC along each leg are fitted by

$$n(r) = N_0 r^\mu e^{-\lambda r}, \quad (4)$$

where  $r$  is the droplet radius,  $n(r)$  is the number concentration for each bin with radius of  $r$ , and  $N_0$ ,  $\lambda$ , and  $\mu$  are three parameters. In the construction of initial droplet size distribution, only the mean value (20.4) and

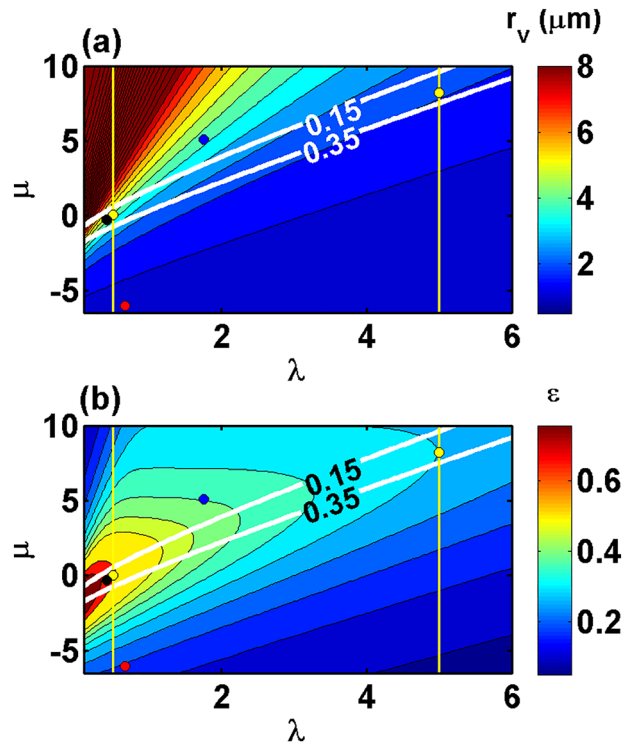


**Figure 13.** (a) Volume-mean radius ( $r_v$ ) as a function of parameters ( $\mu$  and  $\lambda$ ) in the gamma size distributions (equation 4). (b) Relative dispersion ( $\epsilon$ ) of cloud droplet size distribution as a function of  $\mu$  and  $\lambda$ . The yellow dots represent the scenarios where the correlation of  $\epsilon$  versus  $r_v$  changes from positive to negative with increasing  $\mu$  for  $\lambda = 5$  and  $0.5$  (the yellow lines), respectively. The black, red, and blue dots represent the fitting results of mean droplet size distributions in fog (Figure 12b), cloud with  $r_v \leq 2.2 \mu\text{m}$ , and cloud with  $r_v > 2.2 \mu\text{m}$  (Figure 1b), respectively. The two white contours represent first bin strength.

standard deviation (7.46) of  $\mu$  from the fitting equations are used;  $N_0$  and  $\lambda$  are calculated to meet the conditions of adiabatic LWC of  $0.46 \text{ g m}^{-3}$ ,  $n_c$  of  $1332.6 \text{ cm}^{-3}$ , and  $r_v$  of  $4.35 \mu\text{m}$  with equations ((A4), (A6), and (A8)). Figure 11 shows that the results assuming gamma distribution are similar to those with a fixed droplet size shown above. Therefore, the conclusions reached by the EMPM simulations are robust.

### 3.3 Further Discussions

Another interesting point is that the hypothesis can be further supported by observational data of eight fog events, collected in Nanjing ( $32^\circ 12' \text{N}$ ,  $118^\circ 42' \text{E}$ ; 22 m above sea level), China, during the winter of 2007 (Liu et al., 2012; Niu et al., 2012). Fog droplets from  $0.5$  to  $25 \mu\text{m}$  (radius) in 20 bins were measured with a droplet spectrometer (FM-100) at 1 Hz. Only the droplets within the range of  $1$  to  $25 \mu\text{m}$  (radius) are used to calculate microphysical properties (Niu et al., 2010). As an example, Figure 12 shows a case from 16:37 Beijing Standard Time (BST = Universal Time Coordinated + 8 hr) on 19 December to 16:11 BST on 20 December 2007. The results in other cases are similar. As shown in Figure 12, like the  $r_v \leq 2.2 \mu\text{m}$  group for the cumulus clouds,  $\epsilon$  and  $r_v$  are positively correlated; the mean fog droplet size distribution has the peak at the first bin, and FBS is 0.60, even larger than that for  $r_v \leq 2.2 \mu\text{m}$  in Figure 1b. Since the correlation is always positive, here the maximum  $r_v$  (around  $8 \mu\text{m}$ ) is taken to be the transitional  $r_v$ , much larger than  $2.2 \mu\text{m}$  in RACORO.

The different values of transitional  $r_v$  can be further examined by analyzing the role of truncated gamma droplet size distribution in view of its popular use in describing cloud droplet size distributions (e.g., Liu et al., 2002). Because droplets in the range of  $1$  to  $25 \mu\text{m}$  (radius) are often taken to be cloud droplets, a truncated gamma distribution from  $1$  to  $25 \mu\text{m}$  is employed to study the correlation between  $\epsilon$  and  $r_v$ , when  $\lambda$  and  $\mu$  vary. See Appendix A for the equations of  $\epsilon$  and  $r_v$ . As expected, Figure 13 shows that both  $\mu$  and  $\lambda$  are critical to the correlation of  $\epsilon$  versus  $r_v$ . When  $\mu$  is larger than 0, the correlation of  $\epsilon$  versus  $r_v$  mainly changes

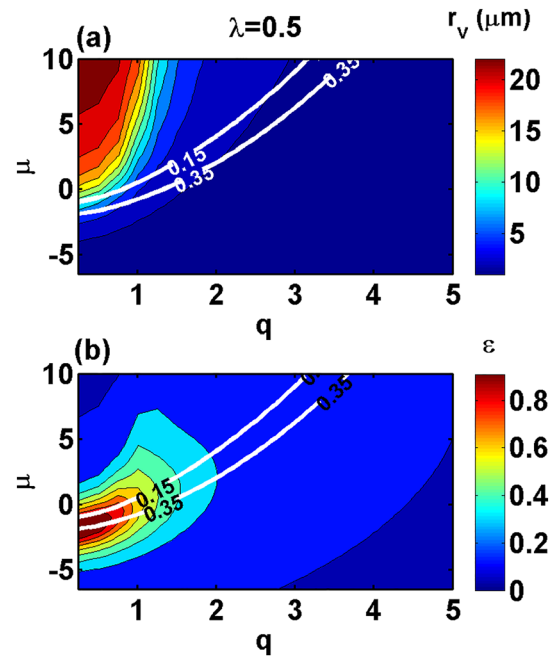


**Figure 14.** (a) Volume-mean radius ( $r_v$ ) as a function of two parameters ( $\mu$ ,  $q$ ) in the modified gamma size distributions (equation 5). (b) Relative dispersion ( $\epsilon$ ) of cloud droplet size distribution as a function of  $\mu$  and  $q$ . The parameter ( $\lambda$ ) is set to be 0.5. The two white contours represent first bin strength.

from positive to negative with decreasing  $\lambda$ . However, when  $\mu$  is smaller than 0, the correlation is mainly positive with varying  $\lambda$ . For a given  $\lambda$ , the correlation always changes from positive to negative with increasing  $\mu$ , but the transitional  $r_v$  is different for different values of  $\lambda$ . For  $\lambda$  varying from 5 to 0.5 (the yellow lines), the transitional  $r_v$  (the yellow dots) increases from 2.1 to 4.3  $\mu\text{m}$ ; at the same time,  $\mu$  decreases. When  $\mu$  further decreases to be smaller than 0, as mentioned above, the correlation of  $\epsilon$  versus  $r_v$  is positive, and the transitional  $r_v$  can reach 6  $\mu\text{m}$  or even larger, as  $\lambda$  decreases.

With Figure 13, the different behaviors of  $\epsilon$  versus  $r_v$  in the fog and two groups of cloud samples can be reconciled. The mean fog and cloud droplet size distributions are fitted by gamma distributions, and the parameters of the fitting equations are shown in Figure 13. Both the fog droplet size distributions and the cloud droplet size distributions with  $r_v \leq 2.2 \mu\text{m}$  have negative  $\mu$ , and therefore,  $\epsilon$  and  $r_v$  are positively correlated; compared with these cloud droplet size distributions with  $r_v \leq 2.2 \mu\text{m}$ , the fog droplet size distributions have larger  $\mu$  and smaller  $\lambda$ , which corresponds to larger transitional  $r_v$ . This could be a reason why the fog always exhibits a positive correlation, whereas the cloud has the transitional  $r_v$  around 2.2  $\mu\text{m}$ . Physically, the phenomenon in fog is likely related to very high interstitial aerosol number concentration with radius close to 1  $\mu\text{m}$  and low supersaturation. Although the data in the range of 0.5–1  $\mu\text{m}$  (radius) are often thought to be noisy, they can still give some hints (Lu et al., 2013). The number concentration in this bin is much higher than that at the current peak in the radius range of 1–2  $\mu\text{m}$  (figure not shown). Shen et al. (2018) estimated that supersaturation in their fog cases was generally lower than 0.04%. Because of low supersaturation, only a small fraction of aerosols can be activated and they grow slowly. The cutoff between droplets and interstitial aerosols becomes important to affect the relationship between  $\epsilon$  versus  $r_v$ . This conclusion needs to be further substantiated when better and more comprehensive data sets are available. Unlike this, in the cumulus clouds, condensation with continuous new activation of droplets mainly occurs near the cloud base where  $r_v$  is small. That could be a physical reason why the correlation between  $\epsilon$  and  $r_v$  is positive only for  $r_v \leq 2.2 \mu\text{m}$  in the cumulus clouds but continuously positive even when  $r_v$  reaches  $\sim 8 \mu\text{m}$  in the fogs. For the cloud droplet size distributions with  $r_v > 2.2 \mu\text{m}$ ,  $\mu$  is positive; condensation is the dominant process, as discussed in Liu et al. (2008).

Besides gamma distribution, the modified gamma distribution is also examined

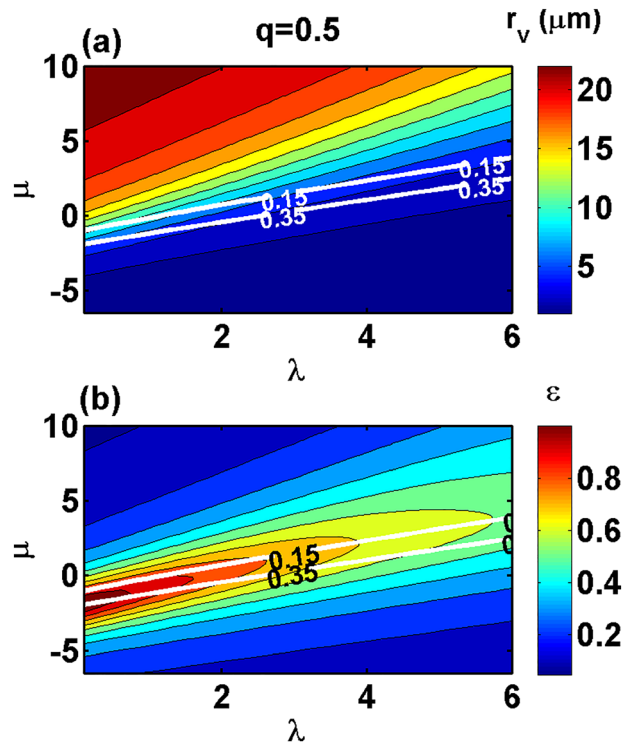


**Figure 15.** (a) Volume-mean radius ( $r_v$ ) as a function of two parameters ( $\mu$ ,  $\lambda$ ) in the modified gamma size distributions (equation 5). (b) Relative dispersion ( $\epsilon$ ) of cloud droplet size distribution as a function of  $\mu$  and  $\lambda$ . The parameter ( $q$ ) is set to be 0.5. The two white contours represent first bin strength.

$$n(r) = N_0 r^\mu e^{-\lambda r^q}, \quad (5)$$

where  $q$  is the fourth parameter. This four-parameter distribution covers both gamma distribution and Weibull distribution as special cases. The results (Figures 14 and 15) are similar to those for the gamma distribution and support the conjecture as well. In addition, contours of FBS in Figures 13–15 show that the sign change points of  $\epsilon$  versus  $r_v$  with maximum  $\epsilon$  are well between the contours of 0.15 and 0.35. The range of 0.15–0.35 can also separate the positive and negative correlations in the adiabatic parcel model and EMPM simulations (Figures 2–4 and 7–9). FBS in the RACORO clouds is 0.54 for the positive correlation of  $\epsilon$  versus  $r_v$  and 0.03 for the negative correlation (Figure 1b); FBS in the Nanjing fog event is 0.60 for the positive correlation (Figure 12b). Therefore, theoretical, numerical, and observational results all support that 0.15–0.35 could be the critical FBS at the sign change points. More studies are needed to quantify the relationship between FBS and the relationship of  $\epsilon$  versus  $r_v$ . This quantity will be useful in future studies. It would be more convenient to calculate FBS to estimate the relationship between  $\epsilon$  and  $r_v$  in analyzing cloud microphysics observations or bin microphysics simulations. Currently, gamma distribution with radius from 0 to  $\infty$  is often assumed in bulk microphysics schemes. If truncated gamma distribution is assumed, FBS could be also helpful. Furthermore, application of FBS is not limited to cloud droplet size distribution. This quantity can be used, as long as a distribution can be described by gamma or modified gamma distribution, for example, size distributions of rain, graupel, and snow.

#### 4. Concluding Remarks

Analysis of microphysical measurements collected in the cumulus clouds during RACORO shows a nonmonotonic relationship between  $\epsilon$  and  $r_v$ :  $\epsilon$  is positively correlated with  $r_v$  when  $r_v \leq 2.2 \mu\text{m}$  and negatively correlated with  $r_v$  when  $r_v > 2.2 \mu\text{m}$ . The positive correlation for small  $r_v$  is expected, since both  $\epsilon$  and  $r_v$  are small when clouds are newly born. Based on the result, it is hypothesized that whether or not condensation (evaporation) occurs simultaneously with a large number of newly activated (deactivated) droplets determines the sign of the correlation between  $\epsilon$  and  $r_v$ .

The hypothesis is substantiated by use of numerical simulations with activation intensity, deactivation intensity, and a newly defined quantity (FBS). An adiabatic parcel model is used to examine the correlation between  $\varepsilon$  and  $r_v$  in the formation and growth processes in clouds. The correlation changes from positive to negative when a cloud parcel moves upward from cloud base. From the cloud base to the transitional point of correlation coefficient sign change, condensation occurs with a large number of newly formed droplets; above the transitional point, condensation occurs without newly formed droplets, consistent with the hypothesis. The EMPM is used to study the correlation between  $\varepsilon$  and  $r_v$  in the isobaric entrainment-mixing processes. The correlation changes from negative to positive as the mixing and evaporation proceeds (i.e.,  $r_v$  decreases). At the beginning of evaporation, evaporation occurs without a large number of droplets deactivated; thus,  $\varepsilon$  and  $r_v$  are negatively correlated; when evaporation proceeds, more and more droplets are deactivated, and  $\varepsilon$  and  $r_v$  become positively correlated. In both simulations with the adiabatic and EMPM parcel models, the positive correlation between  $\varepsilon$  and  $r_v$  corresponds to large FBS, deactivation intensity, or activation intensity, which tends to cause the peak of cloud droplet size distribution at the first bin; the negative correlation corresponds to small FBS, deactivation intensity, or activation intensity, which tends to cause the peak at the middle of cloud droplet size distribution. The critical FBS dividing positive and negative correlations is 0.15–0.35.

The fog observations in Nanjing, China, also support the hypothesis. There is a positive correlation between  $\varepsilon$  and  $r_v$ , and the peaks of droplet size distributions are always at the first bin. The reason is that a large number of haze particles are readily available for activation along with condensational growth of fog droplets. In addition, assuming that cloud droplet size distribution follows truncated gamma distribution, the correlation between  $\varepsilon$  and  $r_v$  changes from positive to negative with increasing  $r_v$  and the transitional  $r_v$  increases with decreasing  $\mu$  and  $\lambda$ ; when  $\mu$  further decreases to be negative, the correlation is always positive. This theoretical understanding reconciles the different behaviors of  $\varepsilon$  versus  $r_v$  in the fog and two groups of cloud droplet size distributions. Assuming modified gamma distribution also supports the above conclusion.

This study suggests that it is critical to consider the concurrent occurrence of activation and condensational growth, or deactivation and evaporation, in study of aerosol-cloud interactions. Homogeneous/inhomogeneous entrainment-mixing mechanisms are also expected to affect  $\varepsilon$ ,  $r_v$ , and their relationship. In reality, entrainment-mixing mechanisms are often between the two extreme mechanisms, which usually increases  $\varepsilon$  and decreases  $r_v$ , compared with adiabatic values. Although entrainment-mixing mechanisms are not discussed in detail, different mechanisms are already included because different conditions (droplet size, dissipation rate, relative humidity in environment, and dry air fraction) are assumed in section 3.2. Furthermore, the key processes affecting the relationship of  $\varepsilon$  versus  $r_v$  (e.g., droplet activation and deactivation) frequently occur near cloud boundaries where separation between clouds and aerosols becomes murky. Therefore, understanding of the  $\varepsilon$  versus  $r_v$  relationship likely sheds new light on the so-called “twilight zone” between cloudy and cloud-free air as well, which in turn affects evaluation of aerosol-cloud interactions and retrieval of aerosol optical depth (e.g., Chiu et al., 2009; Koren et al., 2007; Schwarz et al., 2017; Varnai & Marshak, 2011).

Several points are noteworthy. First, the conclusions in this study are valid under different  $w$  conditions in the observations and simulations; however, the detailed effect of  $w$  fluctuations merits further inspection. Second, also merits special attention is the fact that cloud edge regions have been likely significantly under-sampled due to aircraft sampling bias toward cloud cores and probe measurement uncertainties. Third, the ratio of  $n_c$  to cloud condensation nuclei concentration could serve as a good measure of activation. The ratio's impact on the relationship between  $\varepsilon$  and  $r_v$  deserves further examination.

## Appendix A: Derivations of the Moments in Gamma Size Distribution

Gamma size distribution is

$$n(r) = N_0 r^\mu e^{-\lambda r}, \quad (\text{A1})$$

where  $r$  and  $n(r)$  are the droplet radius and the number of droplets per unit volume per unit radius interval, respectively;  $N_0$ ,  $\lambda$ , and  $\mu$  are three parameters. For the truncated size distribution, the

radius is in the range of 1–25  $\mu\text{m}$ . The normalized first, second, and third moments of the gamma size distribution are

$$m_1 = \lambda^{-1}(\mu + 1) \frac{P(25\lambda, \mu + 2) - P(\lambda, \mu + 2)}{P(25\lambda, \mu + 1) - P(\lambda, \mu + 1)}, \quad (\text{A2})$$

$$m_2 = \lambda^{-2}(\mu + 2)(\mu + 1) \frac{P(25\lambda, \mu + 3) - P(\lambda, \mu + 3)}{P(25\lambda, \mu + 1) - P(\lambda, \mu + 1)}, \quad (\text{A3})$$

$$m_3 = \lambda^{-3}(\mu + 3)(\mu + 2)(\mu + 1) \frac{P(25\lambda, \mu + 4) - P(\lambda, \mu + 4)}{P(25\lambda, \mu + 1) - P(\lambda, \mu + 1)}, \quad (\text{A4})$$

respectively. In equations ((A2)–(A4)),  $P(x, a)$  is incomplete gamma function:

$$P(x, a) = \frac{1}{\Gamma(a)} \int_0^x e^{-t} t^{a-1} dt, \quad (\text{A5})$$

where  $x$  and  $a$  are two parameters;  $\Gamma$  is complete gamma function. With the moments,  $r_v$  and  $\varepsilon$  can be calculated as follows:

$$r_v = m_3^{1/3}, \quad (\text{A6})$$

$$\varepsilon = \frac{(m_2 - m_1^2)^{1/2}}{m_1}, \quad (\text{A7})$$

respectively. The cloud droplet number concentration ( $n_c$ ) is

$$n_c = \frac{N_0 \Gamma(\mu + 1)}{\lambda^{\mu+1}} [P(25\lambda, \mu + 1) - P(\lambda, \mu + 1)]. \quad (\text{A8})$$

#### Acknowledgments

We appreciate the helpful discussion about the instruments with Drs. Darrel Baumgardner and Fan Mei. This research is supported by the National Key Research and Development Program of China (2017YFA0604001), the Natural Science Foundation of Jiangsu Province (BK20160041), the National Natural Science Foundation of China (41822504, 41975181, and 91537108), the Qinglan Project (R2018Q05), and the Six Talent Peak Project in Jiangsu (2015-JY-011). Liu is supported by the U.S. Department of Energy Office of Science Biological and Environmental Research as part of the Atmospheric Systems Research (ASR) Program and Solar Energy and Technology Office (SETO). Brookhaven National Laboratory is operated by Battelle for the U.S. Department of Energy under Contract DE-SC00112704. Yum is supported by the National Research Foundation of Korea (NRF) grant funded by the Korea Government (MSIT) (NRF-2018R1A2B2006965). Chen is supported by the U.S. Department of Energy Office of Science Biological and Environmental Research as part of the Atmospheric Systems Research (ASR) Program. Pacific Northwest National Laboratory is operated by Battelle for the U.S. Department of Energy under Contract DE-AC05-76RLO1830. The RACORO data are available online (<https://www.arm.gov/research/campaigns/aaf2009racoro>). The fog data and cloud numerical simulations are available online ([https://figshare.com/articles/data\\_submitted\\_2019JD031868\\_zip/12085503](https://figshare.com/articles/data_submitted_2019JD031868_zip/12085503)).

#### References

- Anal Kumar, V., Pandithurai, G., Leena, P. P., Dani, K. K., Murugavel, P., Sonbawne, S. M., et al. (2016). Investigation of aerosol indirect effects on monsoon clouds using ground-based measurements over a high-altitude site in Western Ghats. *Atmospheric Chemistry and Physics*, 16(13), 8423–8430.
- Baumgardner, D. (2020). Personal communication on the CAS observation.
- Baumgardner, D., Jonsson, H., Dawson, W., O'Connor, D., & Newton, R. (2001). The cloud, aerosol and precipitation spectrometer: A new instrument for cloud investigations. *Atmospheric Research*, 59–60, 251–264.
- Beals, M. J., Fugal, J. P., Shaw, R. A., Lu, J., Spuler, S. M., & Stith, J. L. (2015). Holographic measurements of inhomogeneous cloud mixing at the centimeter scale. *Science*, 350(6256), 87–90. <https://doi.org/10.1126/science.aab0751>
- Bera, S., Prabha, T. V., & Grabowski, W. W. (2016). Observations of monsoon convective cloud microphysics over India and role of entrainment-mixing. *Journal of Geophysical Research: Atmospheres*, 121, 9767–9788. <https://doi.org/10.1002/2016JD025133>
- Chandrakar, K. K., Cantrell, W., Chang, K., Ciochetto, D., Niedermeier, D., Ovchinnikov, M., et al. (2016). Aerosol indirect effect from turbulence-induced broadening of cloud-droplet size distributions. *Proceedings of the National Academy of Sciences of the United States of America*, 113(50), 14,243–14,248.
- Chandrakar, K. K., Cantrell, W., & Shaw, R. A. (2018). Influence of turbulent fluctuations on cloud droplet size dispersion and aerosol indirect effects. *Journal of the Atmospheric Sciences*, 75(9), 3191–3209. <https://doi.org/10.1175/jas-d-18-0006.1>
- Chen, J., Liu, Y., Zhang, M., & Peng, Y. (2016). New understanding and quantification of the regime dependence of aerosol-cloud interaction for studying aerosol indirect effects. *Geophysical Research Letters*, 43, 1780–1787. <https://doi.org/10.1002/2016GL067683>
- Chen, J., Liu, Y., Zhang, M., & Peng, Y. (2018). Height dependency of aerosol-cloud interaction regimes. *Journal of Geophysical Research: Atmospheres*, 123, 491–506. <https://doi.org/10.1002/2017JD027431>
- Chiu, J. C., Marshak, A., Knyazikhin, Y., Pilewski, P., & Wiscombe, W. J. (2009). Physical interpretation of the spectral radiative signature in the transition zone between cloud-free and cloudy regions. *Atmospheric Chemistry and Physics*, 9(4), 1419–1430. <https://doi.org/10.5194/acp-9-1419-2009>
- Clothiaux, E. E., Ackerman, T. P., Mace, G. G., Moran, K. P., Marchand, R. T., Miller, M. A., & Martner, B. E. (2000). Objective determination of cloud heights and radar reflectivities using a combination of active remote sensors at the ARM CART sites. *Journal of Applied Meteorology*, 39(5), 645–665.
- Deng, Z., Zhao, C., Zhang, Q., Huang, M., & Ma, X. (2009). Statistical analysis of microphysical properties and the parameterization of effective radius of warm clouds in Beijing area. *Atmospheric Research*, 93(4), 888–896. <https://doi.org/10.1016/j.atmosres.2009.04.011>
- Desai, N., Chandrakar, K. K., Chang, K., Cantrell, W., & Shaw, R. A. (2018). Influence of microphysical variability on stochastic condensation in a turbulent laboratory cloud. *Journal of the Atmospheric Sciences*, 75(1), 189–201. <https://doi.org/10.1175/jas-d-17-0158.1>
- Desai, N., Glienne, S., Fugal, J., & Shaw, R. A. (2019). Search for microphysical signatures of stochastic condensation in marine boundary layer clouds using airborne digital holography. *Journal of Geophysical Research: Atmospheres*, 124, 2739–2752. <https://doi.org/10.1029/2018jd029033>

- Diskin, G. S., Podolske, J. R., Sachse, G. W., & Slate, T. A. (2002). *Open-path airborne tunable diode laser hygrometer, paper presented at proceedings of SPIE*. WA, USA: Seattle.
- Fast, J. D., Berg, L. K., Alexander, L., Bell, D., D'Ambro, E., Hubbe, J., et al. (2019). Overview of the HI-SCALE field campaign: A new perspective on shallow convective clouds. *Bulletin of the American Meteorological Society*, *100*(5), 821–840. <https://doi.org/10.1175/bams-d-18-0030.1>
- Gerber, H. E., Frick, G. M., Jensen, J. B., & Hudson, J. G. (2008). Entrainment, mixing, and microphysics in trade-wind cumulus. *Journal of the Meteorological Society of Japan*, *86A*, 87–106.
- Howell, W. E. (1949). The growth of cloud drops in uniformly cooled air. *Journal of Meteorology*, *6*(2), 134–149.
- Hsieh, W. C., Jonsson, H., Wang, L. P., Buzorius, G., Flagan, R. C., Seinfeld, J. H., & Nenes, A. (2009). On the representation of droplet coalescence and autoconversion: Evaluation using ambient cloud droplet size distributions. *Journal of Geophysical Research*, *114*, D07201. <https://doi.org/10.1029/2008JD010502>
- Koren, I., Remer, L. A., Kaufman, Y. J., Rudich, Y., & Martins, J. V. (2007). On the twilight zone between clouds and aerosols. *Geophysical Research Letters*, *34*, L08805. <https://doi.org/10.1029/2007gl029253>
- Krueger, S., Su, C., & McMurtry, P. (1997). Modeling entrainment and finescale mixing in cumulus clouds. *Journal of the Atmospheric Sciences*, *54*, 2697–2712. [https://doi.org/10.1175/1520-0469\(1997\)054<2697:MEAFMI>2.0.CO;2](https://doi.org/10.1175/1520-0469(1997)054<2697:MEAFMI>2.0.CO;2)
- Krueger, S. K. (2008). *Fine-scale modeling of entrainment and mixing of cloudy and clear air, paper presented at the 15th international conference on clouds and precipitation*. Mexico: Cancun.
- Kumar, B., Schumacher, J., & Shaw, R. A. (2014). Lagrangian mixing dynamics at the cloudy–clear air interface. *Journal of the Atmospheric Sciences*, *71*(7), 2564–2580. <https://doi.org/10.1175/JAS-D-13-0294.1>
- Li, Z., Rosenfeld, D., & Fan, J. (2017). Aerosols and their impact on radiation, clouds, precipitation, and severe weather events. *Oxford Research Encyclopedias*. <https://doi.org/10.1093/acrefore/9780199389414.013.126>
- Liu, D., Niu, S., Yang, J., Zhao, L., Lü, J., & Lu, C. (2012). Summary of a 4-year fog field study in northern Nanjing, part 1: Fog boundary layer. *Pure and Applied Geophysics*, *169*(5–6), 809–819. <https://doi.org/10.1007/s00024-011-0343-x>
- Liu, Y., Daum, P., Guo, H., & Peng, Y. (2008). Dispersion bias, dispersion effect, and the aerosol–cloud conundrum. *Environmental Research Letters*, *3*, 045021.
- Liu, Y., & Daum, P. H. (2002). Anthropogenic aerosols: Indirect warming effect from dispersion forcing. *Nature*, *419*(6907), 580–581. <https://doi.org/10.1038/419580a>
- Liu, Y., Daum, P. H., Chai, S. K., & Liu, F. (2002). Cloud parameterizations, cloud physics, and their connections: An overview, Recent Res. Devel. *Geophysics*, *4*, 119–142.
- Liu, Y., Daum, P. H., & McGraw, R. (2004). An analytical expression for predicting the critical radius in the autoconversion parameterization. *Geophysical Research Letters*, *31*, L06121. <https://doi.org/10.1029/2003gl019117>
- Liu, Y., Daum, P. H., McGraw, R., & Miller, M. (2006). Generalized threshold function accounting for effect of relative dispersion on threshold behavior of autoconversion process. *Geophysical Research Letters*, *33*, L11804. <https://doi.org/10.1029/2005gl025500>
- Liu, Y., Daum, P. H., McGraw, R. L., Miller, M. A., & Niu, S. (2007). Theoretical expression for the autoconversion rate of the cloud droplet number concentration. *Geophysical Research Letters*, *34*, L16821. <https://doi.org/10.1029/2007gl030389>
- Liu, Y., Daum, P. H., & Yum, S. S. (2006). Analytical expression for the relative dispersion of the cloud droplet size distribution. *Geophysical Research Letters*, *33*, L02810. <https://doi.org/10.1029/2005GL024052>
- Lu, C., Liu, Y., Niu, S., & Vogelmann, A. M. (2012a). Lateral entrainment rate in shallow cumuli: Dependence on dry air sources and probability density functions. *Geophysical Research Letters*, *39*, L20812. <https://doi.org/10.1029/2012GL053646>
- Lu, C., Liu, Y., Niu, S., & Vogelmann, A. M. (2012b). Observed impacts of vertical velocity on cloud microphysics and implications for aerosol indirect effects. *Geophysical Research Letters*, *39*, L21808. <https://doi.org/10.1029/2012GL053599>
- Lu, C., Liu, Y., Niu, S., & Xue, Y. (2018). Broadening of cloud droplet size distributions and warm rain initiation associated with turbulence: An overview. *Atmospheric and Oceanic Science Letters*, *11*(2), 123–135. <https://doi.org/10.1080/16742834.2018.1410057>
- Lu, C., Liu, Y., Niu, S., Zhao, L., Yu, H., & Cheng, M. (2013). Examination of microphysical relationships and corresponding microphysical processes in warm fogs. *Acta Meteorologica Sinica*, *27*, 832–848.
- Lu, C., Liu, Y., Yum, S. S., Niu, S., & Endo, S. (2012). A new approach for estimating entrainment rate in cumulus clouds. *Geophysical Research Letters*, *39*, L04802. <https://doi.org/10.1029/2011GL050546>
- Lu, C., Liu, Y., Zhu, B., Yum, S. S., Krueger, S. K., Qiu, Y., et al. (2018). On which microphysical time scales to use in studies of entrainment-mixing mechanisms in clouds. *Journal of Geophysical Research: Atmospheres*, *123*, 3740–3756. <https://doi.org/10.1002/2017JD027985>
- Lu, C., Niu, S., Liu, Y., & Vogelmann, A. M. (2013). Empirical relationship between entrainment rate and microphysics in cumulus clouds. *Geophysical Research Letters*, *40*, 2333–2338. <https://doi.org/10.1002/grl.50445>
- Ma, J., Chen, Y., Wang, W., Yan, P., Liu, H., Yang, S., et al. (2010). Strong air pollution causes widespread haze-clouds over China. *Journal of Geophysical Research*, *115*, D18204. <https://doi.org/10.1029/2009jd013065>
- Martin, G. M., Johnson, D. W., & Spice, A. (1994). The measurement and parameterization of effective radius of droplets in warm stratocumulus clouds. *Journal of the Atmospheric Sciences*, *51*(13), 1823–1842. [https://doi.org/10.1175/1520-0469\(1994\)051<1823:TMAPOE>2.0.CO;2](https://doi.org/10.1175/1520-0469(1994)051<1823:TMAPOE>2.0.CO;2)
- McComiskey, A., Feingold, G., Frisch, A. S., Turner, D. D., Miller, M. A., Chiu, J. C., et al. (2009). An assessment of aerosol-cloud interactions in marine stratus clouds based on surface remote sensing. *Journal of Geophysical Research*, *114*, D09203. <https://doi.org/10.1029/2008jd011006>
- McFarquhar, G. M., & Heymsfield, A. J. (2001). Parameterizations of INDOEX microphysical measurements and calculations of cloud susceptibility: Applications for climate studies. *Journal of Geophysical Research*, *106*(D22), 28,675–28,698.
- Niu, S., Liu, D., Zhao, L., Lu, C., Lü, J., & Yang, J. (2012). Summary of a 4-year fog field study in northern Nanjing, part 2: Fog microphysics. *Pure and Applied Geophysics*, *169*(5–6), 1137–1155. <https://doi.org/10.1007/s00024-011-0344-9>
- Niu, S., Lu, C., Liu, Y., Zhao, L., Lü, J., & Yang, J. (2010). Analysis of the microphysical structure of heavy fog using a droplet spectrometer: A case study. *Advances in Atmospheric Sciences*, *27*(6), 1259–1275. <https://doi.org/10.1007/s00376-010-8192-6>
- Pandithurai, G., Dipu, S., Prabha, T. V., Mahes Kumar, R. S., Kulkarni, J. R., & Goswami, B. N. (2012). Aerosol effect on droplet spectral dispersion in warm continental cumuli. *Journal of Geophysical Research*, *117*, D16202. <https://doi.org/10.1029/2011JD016532>
- Pawlowska, H., Grabowski, W. W., & Brenguier, J. L. (2006). Observations of the width of cloud droplet spectra in stratocumulus. *Geophysical Research Letters*, *33*, L19810. <https://doi.org/10.1029/2006GL026841>

- Peng, Y., & Lohmann, U. (2003). Sensitivity study of the spectral dispersion of the cloud droplet size distribution on the indirect aerosol effect. *Geophysical Research Letters*, *30*(10), 1507. <https://doi.org/10.1029/2003gl017192>
- Peng, Y., Lohmann, U., Leaitch, R., & Kulmala, M. (2007). An investigation into the aerosol dispersion effect through the activation process in marine stratus clouds. *Journal of Geophysical Research*, *112*, D11117. <https://doi.org/10.1029/2006jd007401>
- Peters, M. D., & Kreidenweis, S. M. (2007). A single parameter representation of hygroscopic growth and cloud condensation nucleus activity. *Atmospheric Chemistry and Physics*, *7*(8), 1961–1971. <https://doi.org/10.5194/acp-7-1961-2007>
- Podolske, J. R., Sachse, G. W., & Diskin, G. S. (2003). Calibration and data retrieval algorithms for the NASA Langley/Ames diode laser hygrometer for the NASA transport and chemical evolution over the Pacific (TRACE-P) mission. *Journal of Geophysical Research*, *108*(D20), 8792. <https://doi.org/10.1029/2002jd003156>
- Prabha, T. V., Patade, S., Pandithurai, G., Khain, A., Axisa, D., Pradeep-Kumar, P., et al. (2012). Spectral width of premonsoon and monsoon clouds over Indo-Gangetic valley. *Journal of Geophysical Research*, *117*, D20205. <https://doi.org/10.1029/2011JD016837>
- Rogers, R. R., & Yau, M. K. (1989). *A short course in cloud physics*. Burlington, MA, USA: Butterworth Heinemann.
- Rotstain, L. D., & Liu, Y. (2003). Sensitivity of the first indirect aerosol effect to an increase of cloud droplet spectral dispersion with droplet number concentration. *Journal of Climate*, *16*(21), 3476–3481.
- Rotstain, L. D., & Liu, Y. (2009). Cloud droplet spectral dispersion and the indirect aerosol effect: Comparison of two treatments in a GCM. *Geophysical Research Letters*, *36*, L10801. <https://doi.org/10.1029/2009gl038216>
- Schwarz, K., Cermak, J., Fuchs, J., & Andersen, H. (2017). Mapping the twilight zone—What we are missing between clouds and aerosols. *Remote Sensing*, *9*(6), 577.
- Shen, C., Zhao, C., Ma, N., Tao, J., Zhao, G., Yu, Y., & Kuang, Y. (2018). Method to estimate water vapor supersaturation in the ambient activation process using aerosol and droplet measurement data. *Journal of Geophysical Research: Atmospheres*, *123*, 10,606–10,619. <https://doi.org/10.1029/2018JD028315>
- Small, J. D., Chuang, P., & Jonsson, H. (2013). Microphysical imprint of entrainment in warm cumulus. *Tellus B*, *65*, 6647–6662.
- Su, C.-W., Krueger, S. K., McMurtry, P. A., & Austin, P. H. (1998). Linear eddy modeling of droplet spectral evolution during entrainment and mixing in cumulus clouds. *Atmospheric Research*, *47–48*, 41–58.
- Tas, E., Koren, I., & Altaratz, O. (2012). On the sensitivity of droplet size relative dispersion to warm cumulus cloud evolution. *Geophysical Research Letters*, *39*, L13807. <https://doi.org/10.1029/2012GL052157>
- Tölle, M. H., & Krueger, S. K. (2014). Effects of entrainment and mixing on droplet size distributions in warm cumulus clouds. *Journal of Advances in Modeling Earth Systems*, *6*, 281–299. <https://doi.org/10.1002/2012MS000209>
- Varnai, T., & Marshak, A. (2011). Global CALIPSO observations of aerosol changes near clouds. *IEEE Geoscience and Remote Sensing Letters*, *8*(1), 19–23. <https://doi.org/10.1109/LGRS.2010.2049982>
- Vogelmann, A. M., McFarquhar, G. M., Ogren, J. A., Turner, D. D., Comstock, J. M., Feingold, G., et al. (2012). RACORO extended-term aircraft observations of boundary layer clouds. *Bulletin of the American Meteorological Society*, *93*(6), 861–878. <https://doi.org/10.1175/bams-d-11-00189.1>
- Wallace, J., & Hobbs, P. (2006). *Atmospheric science: An introductory survey*. San Diego, California, USA: Academic Press.
- Wang, M., & Penner, J. E. (2010). Cirrus clouds in a global climate model with a statistical cirrus cloud scheme. *Atmospheric Chemistry and Physics*, *10*(12), 5449–5474. <https://doi.org/10.5194/acp-10-5449-2010>
- Wang, X., Xue, H., Fang, W., & Zheng, G. (2011). A study of shallow cumulus cloud droplet dispersion by large eddy simulations. *Acta Oceanologica Sinica*, *25*(2), 166–175. <https://doi.org/10.1007/s13351-011-0024-9>
- Wang, Y., Fan, J., Zhang, R., Leung, L. R., & Franklin, C. (2013). Improving bulk microphysics parameterizations in simulations of aerosol effects. *Journal of Geophysical Research: Atmospheres*, *118*, 5361–5379. <https://doi.org/10.1002/jgrd.50432>
- Wood, R. (2000). Parametrization of the effect of drizzle upon the droplet effective radius in stratocumulus clouds. *Quarterly Journal of the Royal Meteorological Society*, *126*(570), 3309–3324. <https://doi.org/10.1002/qj.49712657015>
- Wood, R., Irons, S., & Jonas, P. R. (2002). How important is the spectral ripening effect in stratiform boundary layer clouds? Studies using simple trajectory analysis. *Journal of the Atmospheric Sciences*, *59*(18), 2681–2693. [https://doi.org/10.1175/1520-0469\(2002\)059<2681:hiitsr>2.0.co;2](https://doi.org/10.1175/1520-0469(2002)059<2681:hiitsr>2.0.co;2)
- Xie, X., & Liu, X. (2011). Effects of spectral dispersion on clouds and precipitation in mesoscale convective systems. *Journal of Geophysical Research*, *116*, D06202. <https://doi.org/10.1029/2010JD014598>
- Xie, X., Liu, X., Peng, Y., Wang, Y., Yue, Z., & Li, X. (2013). Numerical simulation of clouds and precipitation depending on different relationships between aerosol and cloud droplet spectral dispersion. *Tellus B*, *65*(1), 19,054.
- Xie, X., Zhang, H., Liu, X., Peng, Y., & Liu, Y. (2017). Sensitivity study of cloud parameterizations with relative dispersion in CAM5.1: Impacts on aerosol indirect effects. *Atmospheric Chemistry and Physics*, *17*(9), 5877–5892. <https://doi.org/10.5194/acp-17-5877-2017>
- Yum, S. S., & Hudson, J. G. (2005). Adiabatic predictions and observations of cloud droplet spectral broadness. *Atmospheric Research*, *73*(3–4), 203–223. <https://doi.org/10.1016/j.atmosres.2004.10.006>
- Yum, S. S., Wang, J., Liu, Y., Senum, G., Springston, S., McGraw, R., & Yeom, J. M. (2015). Cloud microphysical relationships and their implication on entrainment and mixing mechanism for the stratocumulus clouds measured during the VOCALS project. *Journal of Geophysical Research: Atmosphere*, *120*, 5047–5069. <https://doi.org/10.1002/2014JD022802>
- Zhang, M., Bretherton, C. S., Blossey, P. N., Austin, P. H., Bacmeister, J. T., Bony, S., et al. (2013). CGILS: Results from the first phase of an international project to understand the physical mechanisms of low cloud feedbacks in single column models. *Journal of Advances in Modeling Earth Systems*, *5*, 826–842. <https://doi.org/10.1002/2013MS000246>
- Zhao, C., Tie, X., Brasseur, G., Noone, K. J., Nakajima, T., Zhang, Q., et al. (2006). Aircraft measurements of cloud droplet spectral dispersion and implications for indirect aerosol radiative forcing. *Geophysical Research Letters*, *33*, L16809. <https://doi.org/10.1029/2006gl026653>
- Zhao, C., Zhao, L., & Dong, X. (2019). A case study of stratus cloud properties using in situ aircraft observations over Huanghua, China. *Atmosphere*, *10*(1), 19.